

A simple spatial model for extreme tropical cyclone seas

Ryota Wada^{a,*}, Takuji Waseda^a, Philip Jonathan^{b,c}^a*Department of Ocean Technology, Policy and Environment, the University of Tokyo, Japan.*^b*Shell Projects & Technology, London SE1 7NA, United Kingdom.*^c*Department of Mathematics and Statistics, Lancaster University LA1 4YW, United Kingdom.*

Abstract

We seek to improve estimation of extreme sea state severities offshore Japan. In this tropical cyclone-dominated region, magnitudes of large values of storm severity (significant wave height, H_S) observed at a location of interest are highly dependent on the trajectories of tropical cyclones relative to the location. As a result, a naive estimate for a return value of storm severity at a location of interest corresponding to a long return period, made using a relatively short period of observational or hindcast data, shows unrealistically large spatial variation. To address this issue, we propose a pragmatic statistical representation for cyclone sea state severity in space and time, consisting of (1) an extreme value model for the maximum of storm severity per cyclone (over space and time), and (2) a model for the “exposure” of a location to a random cyclone event. For a particular location, exposure quantifies the maximum storm severity observed during a cyclone event, expressed as a fraction of the storm peak severity (over space and time). Importantly, exposure is quantified per location on an absolute spatial lattice, independent of cyclone path relative to the location. Numerous statistical diagnostic tests are performed to justify that modelling assumptions made are consistent with data. Resulting return value estimates have plausible magnitudes and show plausible spatial variation, and in particular reflect bathymetric and shielding effects of coastlines and islands.

Keywords: Exposure; Extreme; Return value; Spatial; Tropical cyclone;

1. Introduction

Rational and consistent methods are essential to assure reliability of offshore structures, providing a basis for allocation of resources and sustainable asset utility. To achieve this, a precise

*Corresponding author. Email: r_wada@k.u-tokyo.ac.jp

description of extremal environmental conditions is desirable though seldom possible. Since extreme environmental events are rare and random by nature, extrapolation of inferences beyond the period of observation is always necessary for specification of design values. This extrapolation is uncertain due to the environment's inherent natural variability, and lack of knowledge due to limited observations and imperfect models.

Tropical cyclones and hurricanes have low rates of occurrence at a location, and when they occur produce large storm severities over limited spatial domains. Extreme sea states in regions such as the North West Pacific, north-west shelf of Australia and Gulf of Mexico are dominated by cyclone occurrence and proximity to cyclone track ([1], [2], [3]). As a result, sample sizes for estimation for design conditions of storm severity (significant wave height, H_S) tend to be small. Further, "naive" estimates for a return value of storm severity at a single location corresponding to a long return period, made using a relatively short period of observational or hindcast data for that location, show unrealistically large spatial variation. (The reader might like to review Figure 18, which shows 100-year return value estimates using a location-by-location analysis for the region of interest offshore Japan. For a given typhoon, there is small scale variability associated with significant wave height (e.g. [4]), due to directional effects and typhoon transition speed. However, the high spatial variation of return value shown in Figure 18, estimated over a relatively long record, is unrealistic, considering the large-scale Pacific High atmospheric circulations that control typhoon tracks and therefore overall typhoon wave characteristics the area. Further details of the analysis are given in Section 6.) The belief is that the cyclone track distribution, observed over very long periods, will be spatially smoother than that suggested by a short period of observation. As a result, return values of storm severity corresponding to long return periods would also be spatially smoother. The objective of this work is to establish a simple but valid statistical framework for estimation of extreme wave environments with more plausible spatial variation.

Extreme value analysis is the basis for empirical estimation of metocean design values in modern engineering, motivated by known asymptotic forms for the distributions of sample maxima or peaks over threshold. When sample size is large, extreme value models provide good estimates for the tails of distributions. However, sample size is often small and epistemic uncertainties from naive extreme value analysis large. For example, consider extreme value estimates at a single location in some region, for a tropical cyclone environment. Since severe sea states only occur close to cyclones

tracks, the actual number of extreme sea states available as the basis for extreme value analysis at the location is likely to be even smaller than the number of tropical cyclones in the region. The engineering literature contains numerous descriptions of approaches to address this issue using techniques such as spatial pooling [5], cyclone track-shifting [6] and explicit track modelling [7]. Spatial pooling seeks to increase the sample size for analysis by including events from multiple locations in a neighbourhood; this is problematic since a given cyclone event at neighbouring locations produces dependent extremes, violating a basic assumption that independent observations be used. We note however, that the working assumption of independence between observations from different locations, combined with correction techniques such as block-bootstrapping, can provide useful estimates from dependent spatial data. Track-shifting and empirical track modelling produce large numbers of realisations of cyclones over the region, thus increasing sample size; the quality of resulting return value estimates depends on exactly how physically realistic the track-shifting or track modelling algorithms are. The statistics literature provides methods to estimate spatially-dependent extremes using extensions of univariate extreme value theory (e.g. [8], [9]); but these constitute overly complicated models for situations where sample size is small.

The aim of the current work is to provide a simple statistical model for extreme sea state severity appropriate for offshore Japan. The model is motivated by two assumptions. Firstly, we assume that, for a given cyclone, the value of the largest storm severity observed anywhere in the spatial domain of interest for the period of the cyclone, is a random variable with distribution independent of storm track, environmental covariates, space and time. This means that we can isolate the so-called “space-time maximum” storm severity (STM) for each of a number of cyclones, and use the set of STMs to estimate the characteristics of extreme STM appropriate for any cyclone in the spatio-temporal domain of interest. This assumption is a strong one, but we demonstrate that it is reasonable given the available data using standard statistical diagnostic tests. The second assumption made is that the influence of any cyclone, regardless of its track, on the largest storm severity observed at any particular location in the spatial domain (expressed as a fraction of STM for the cyclone) can be quantified using the location’s “exposure” to cyclones. For a given location, exposure is a random variable with distribution independent of cyclone STM and track, environmental covariates and time, estimated empirically. Again, this assumption is shown to be plausible for the current application using diagnostic testing. The distribution of exposure varies

with location; coastal and fetch-restricted areas for example will have lower exposure than locations in open water. Together, the STM-exposure model provides a pragmatic, computationally-efficient means of estimating return values and their uncertainties for environments like offshore Japan. We hope that the model provides a useful and informative tool for metocean engineers.

The format of this paper is follows. We introduce the motivating application in Section 2, and the STM and exposure models in Section 3. Section 4 applies the model to data from Section 2, and Section 5 illustrates some of the diagnostic tests performed to justify modelling assumptions. Section 6 provides a comparison of return value estimates from the simple spatial model with those from independent analyses per location. Conclusions are drawn in Section 7.

Note that inferences are made throughout this work for the characteristics of *storm peak* significant wave height per cyclone event, for single locations of sets thereof. For brevity, this quantity is referred to in the text as either *storm severity* or significant wave height H_S on the understanding it refers to the storm peak characteristic.

2. Motivating application

We focus on the North West Pacific ocean, south of Japan, a region where Japan hopes to develop various offshore resources including wind, current and methane hydrates. The wave climate around Japan is generally calm, except for the occurrences of cyclones. Tropical cyclones, referred to in this region as typhoons, dominate the extreme wave environment. The north eastern region of Japan is also affected by mid-latitude cyclones, but the impact is considered minor compared to typhoons. The frequency of typhoons in the West Pacific region is around 26 per annum. Approximately 11 of these per annum pass within 300km of Japan. Only 2 or 3 typhoons per annum actually pass through the region of interest for this work. Strong wind fields rotating anti-clockwise with radius to maximum wind of the order of 100km [10] cause increasing sea state severity as a cyclone passes. The combined effect of cyclone motion along its track and wind field rotation means that locations to the right of an observer travelling along the cyclone track experience stronger winds and larger waves. The occurrence of extreme waves is highly dependent on track. The location of the largest significant wave height under a typhoon does not coincide with the location of the minimum pressure or the maximum wind speed [11].

[Figure 1 about here.]

A 21-year high-resolution wave re-analysis from Todai WW3 [12] was used here as the source of hourly significant wave height data for the period [1994,2014]. We focus on region referred to as “J02” for the Pacific side of the Japanese mainland with coverage $[27.95^\circ, 36.85^\circ]N \times [130.9375^\circ, 146.0625^\circ]E$ and resolution of $0.05^\circ \times 0.0625^\circ$. Water depth is less than 200m only near to the Japanese mainland in Figure 1, which shows the largest storm peak H_S per location in the hindcast period corresponding to tropical cyclones. The “partly circular” features of H_S contours are caused by the fast transition of cyclone peaks across the spatial domain, given the 1-hour temporal resolution of the hindcast output. The largest value of H_S in the hindcast is approximately 23m. In comparison, note that global hindcast models such as ERA-Interim [13] have broad spatial coverage but lower resolution. Their coarse grid fails to reproduce large waves under severe storms [14, 3]. In this study, we limit ourselves to the analysis of the region illustrated. However, the current methodology can be applied to larger regions provided that underlying assumptions remain valid.

Historical data for tropical cyclone tracks in the region was obtained from the International Best Track Archive for Climate Stewardship (IBTrACS) [15]. IBTrACS merges storm information from various meteorological organisations to create a global best track dataset, including positions, pressures, and wind speeds. The storm category “tropical in nature” corresponds to the Japanese Meteorological Association’s classification for all of tropical depressions, tropical storms, severe tropical storms and typhoons. The extraction procedure is: (a) Identify all tracks of storms assigned tropical in nature within spatial domain $[23^\circ, 60^\circ]N \times [125^\circ, 152^\circ]E$, (b) Record track of storm centre in space and time for each storm identified. A large spatial domain for cyclone identification was set to ensure that all cyclones influencing sea state severity in the J02 region were considered. Figure 2 shows tracks for all storm centres for the period [1994,2014]; many tropical storms pass through the region, but just a small fraction of these are extreme typhoons events.

[Figure 2 about here.]

The cyclone track information from IBTrACS together with storm severities from Todai WW3 are used together to estimate models for STM and exposure, introduced in Section 3.

3. Method

We describe the characteristics of tropical cyclones offshore Japan in terms of a model with two components. The first provides a statistical distribution for the space-time maximum storm

severity of a cyclone. The second characterises the exposure of the wave environment at a particular location to cyclone forcing. We proceed as follows. First, in Section 3.1 we estimate the cumulative distribution function of the space-time maximum STM applicable to the whole spatial domain. Then, for each location in the spatial domain, we estimate the empirical distribution of exposure E in Section 3.2. Finally, in Section 3.3, we combine these distributions to estimate the distribution of storm severity at each location corresponding to an arbitrary cyclone event. Application of the resulting STM-exposure model is outlined in Section 4, and diagnostics supporting the veracity of model assumptions are presented in Section 5.

3.1. Space-time maximum (STM)

The STM of a tropical cyclone is the largest value of significant wave height observed anywhere on the spatial domain during the time period of the cyclone. We isolate a set $\{s_i\}_{i=1}^{n_S}$ STM values for n_S cyclone events from the hindcast data, to characterise the distribution of the STM random variable S . We assume that the distribution extreme values of S is independent of cyclone track, typical environmental covariates, space and time.

We estimate $F_{S|\psi_S}$, the conditional distribution of threshold exceedances of S by extreme value analysis. We assume that occurrences of S above some threshold ψ_S follow a generalised Pareto distribution, the parameters of which are estimated using the *likelihood weighted method* [16]. This approach has been demonstrated to perform relatively well for extreme value analysis of small samples. Note that the full distribution $F_S(s)$ can be estimated using

$$F_S(s) = \begin{cases} F^*(s) & \text{for } s \leq \psi_S \\ \tau + (1 - \tau)F_{S|\psi_S}(s) & \text{otherwise} \end{cases} \quad (1)$$

where F^* is an empirical estimate for the distribution of non-exceedances obtained directly by sorting non-exceedances of threshold ψ_S from the sample, and τ is the non-exceedance probability associated with ψ_S . We use the estimated F_S in combination with the exposure model below.

Note, since S is a spatio-temporal maximum, that all cyclone events contribute to the set $\{s_i\}$. This is not the case for an analysis based on data for a single location impacted by only a subset of cyclones. Provided that modelling assumptions are satisfied, we therefore expect to benefit from this increased sample size.

3.2. Exposure

Hindcast data is used further to characterize the exposure of a location to cyclones, in terms of storm severity at that location expressed as a fraction of STM. Specifically, we estimate the marginal distribution $E(r)$ of exposure E at location r as follows.

Assuming that values $\{h(r_j, t)\}$ of H_S are available for a lattice of n_R spatial locations with coordinates $\{r_j\}_{j=1}^{n_R}$ on some spatial domain \mathcal{R} and times t on temporal domain \mathcal{T}_i for each cyclone, we estimate the distribution of E_j ($= E(r_j)$) for each j empirically using the set $\{e_{ij}\}$, where

$$e_{ij} = \max_{t \in \mathcal{T}_i} \frac{h(r_j, t)}{s_i} \quad (2)$$

where s_i is the corresponding STM value. The sample $\{e_{ij}\}$ of exposures therefore informs us about the maximum fractional influence of each of the cyclone events i at each location j . We can sample from this set to estimate the characteristics of $E(r)$ throughout the spatial domain \mathcal{R} , or use it directly as an empirical estimate the distribution of E at any location of interest.

We assume here that the characteristics of E at a location are independent of STM, cyclone track, environmental covariates and time. These assumptions need to be justified.

Note we do not express exposure relative to the location of the storm peak or cyclone track, as is typically done in spatial modelling of cyclones. Instead, exposure is quantified on an absolute spatial lattice \mathcal{R} . The impact of tropical cyclones on waves near the coast is strongly affected by fetch limitation, shielding and shallow water effects. These are all captured naturally by exposure as outlined here. Provided that modelling assumptions are justified, we therefore expect the combination of STM and exposure to provide a useful model for severe tropical cyclone sea states. Note further that the sample $\{e_{ij}\}$ is informative for the spatial structure of $E(r)$ for $r \in \mathcal{R}$. In the current work, we choose only to consider the marginal characteristics of exposure given a location of interest.

3.3. The STM-E model

We use the estimated distribution F_S for STM and the empirical distribution F_{E_j} for E_j at location j to estimate the distribution F_{H_j} of storm severity H_j at location j corresponding to an arbitrary cyclone event, as follows. Since $H_j = E_j \times S$, we can write the cumulative distribution

of H_j as

$$\begin{aligned}
F_{H_j}(h) &= \mathbb{P}(H_j \leq h) \\
&= \int_s \mathbb{P}(E_j S \leq h | S = s) f_S(s) ds \\
&= \int_s \mathbb{P}(E_j \leq h/s) f_S(s) ds \\
&= \int_s F_{E_j}(h/s) f_S(s) ds
\end{aligned} \tag{3}$$

where the final integral can be evaluated simply using numerical integration (e.g. [17]). It is clear from these equations that the largest values of storm severity at a location are not always associated with the largest STMs, but rather with smaller STMs having large exposure E . For convenience, we refer to the STM-exposure model henceforth as STM-E.

3.4. N -year maximum and N -year event

Knowledge of F_{H_j} for location j , together with the assumption that the rate of occurrence of cyclone events is Poisson-distributed with annual rate of occurrence λ , permits us to estimate the distribution $F_{H_j;N}$ of the N -year maximum storm severity (e.g. [2]) at location j using

$$\begin{aligned}
F_{H_j;N}(h) &= \sum_{k=0}^{\infty} \mathbb{P}(k \text{ events in } N \text{ years}) F_{H_j}^k(h) \\
&= \sum_{k=0}^{\infty} \frac{\lambda^k e^{-\lambda}}{k!} F_{H_j}^k(h) \\
&= \exp[-N\lambda(1 - F_{H_j}(h))] \quad .
\end{aligned} \tag{4}$$

Then, the “ N -year event” (or “ N -year return value”) $h_{j;N}$ is then defined as the fractile of the distribution of the annual maximum (setting “ $N=1$ ” in Equation (4) above) with probability $1-1/N$. That is

$$\begin{aligned}
F_{H_j;1}(h_{j;N}) &= \exp[-\lambda(1 - F_{H_j}(h))] \\
&= 1 - \frac{1}{N} \quad .
\end{aligned} \tag{5}$$

The distribution of the N -year maximum is useful since it quantifies the (often very large) uncertainty in the largest value seen in N years. The N -year return value is useful because it provides a single number to quantify the magnitude of extreme events. Both quantities are used below.

4. Application

Here we apply the method from Section 3 to the data from the North West Pacific ocean described in Section 2. As mentioned above, severe storms in Japanese waters in general can also be caused by mid-latitude cyclones. However, on the spatial domain of this study, mid-latitude cyclones are less influential and are therefore not considered; the analysis of course could be extended to include these events. We proceed by estimating an extreme value model for STM (the maximum significant wave height under the typhoon, defined in Section 3) and an empirical distribution for exposure per spatial location. Then we combine these to produce spatial maps for the 100-year return value of H_S , and assess the variability in the value of the 100-year maximum H_S .

4.1. Storm peak events

For a given hindcast grid location, peaks over threshold of H_S are extracted using the peak-picking algorithm [18] for a 3m threshold and storm merging interval of 1.5 days. The results of a sensitivity study into threshold and interval choice will be discussed later in Section 5. Then, we allocate peak over threshold events occurring within the time interval of a particular cyclone to that cyclone, retaining the largest peak in the event of multiple occurrences. When there are multiple tropical cyclones, and for each grid location, the distance to each cyclone track is used as an indicator to associate STM per location to the tropical cyclone with smaller distance. We note that, for each tropical cyclone period (plus an additional 24 hours after the cyclone period) per location we capture the full time-series of significant wave height. This time-series includes the peak of the tropical cyclone and its local evolution, and therefore also captures the largest waves in the tropical cyclone. We repeat this procedure for all locations and compile the sample $\{h_{ij}\}_{i,j=1}^{n_S, n_R}$ of spatial storm peak values for $n_S = 63$ cyclones at n_R locations in 21 years. An example of the spatial distribution of peak H_S for a single cyclone event during September 1996 is shown in Figure 3.

[Figure 3 about here.]

4.2. Space Time Maxima

For each cyclone i in turn, we extract the largest value of $\{h_{ij}\}_{j=1}^{n_R}$, set it equal to STM s_i for that cyclone, and accumulate the set $\{s_i\}_{i=1}^{n_S}$.

As an initial diagnostic, we also record the spatial locations at which each STM occurs. These are shown, together with the magnitude of STM, in Figure 4. There is no obvious spatial dependence between STM and location; we investigate this characteristic further in Section 5. As shown in Figure 4, several STM events occur on the boundary of the region; it might well be that these correspond to cyclones with even larger values of H_S outside the domain. The effect of domain choice on return values is discussed in Section 5.4.

[Figure 4 about here.]

Next, the tail of the distribution for STM is estimated using sample $\{s_i\}$ and the likelihood weighted method [16]. This provides an estimate for the posterior predictive distribution F_S of STM. Figure 5 illustrates the fit obtained, and the joint posterior parameter distribution for generalised Pareto shape ξ and (logarithm of) scale σ . The mode of the distribution corresponds to slightly negative ξ . In this work, we choose to use the likelihood weighted method for inference with STM-E, because of our favorable past experiences with the approach for analysis of samples of Japanese tropical cyclones. However, we note that STM-E approach can be used with other estimation methods.

[Figure 5 about here.]

We note that the distribution of STM is influenced by a large H_s value ($H_s=22.84\text{m}$) in the hindcast. Although the large value exceeds the highest observed H_S , we have assumed it to be trustworthy for the purposes of the current work.

4.3. Exposure

The empirical distribution of exposure E at location j is estimated from the sample $\{e_{ij}\}_{i=1}^{n_S}$ obtained from $\{h_{ij}\}_{i=1}^{n_S}$ as explained in Section 3. Figure 6 shows exposure spatially for six typical tropical cyclones events together with cyclone track. E is large near the track and to the right of track in the direction of propagation as noted in Section 2.

[Figure 6 about here.]

4.4. Return values

[Figure 7 about here.]

Using the estimated STM and exposure distributions as described in Section 3, return value distributions can be estimated. Figure 7 shows the distribution of a single tropical cyclone storm peak H_S for a location P2 (see Figure 8) using the STM-E method, the distribution of a single STM, together with the corresponding distributions for the 100-year maximum H_S at P2 (again using STM-E), and the 100-year maximum STM using Equation (4). Figure 8 shows a spatial map of the 100-year return value estimated using Equation (5).

[Figure 8 about here.]

Accumulated knowledge from studying the ocean environment suggests that the severity of storms is regulated by physical features such as water depth, proximity to land, and land-shadow effects. We judge that Figure 8 and Figure 9 show smooth reduction in H_S as the coast is approached, and smooth reduction around islands, with typical land-shadow effects, consistent with intuition.

[Figure 9 about here.]

4.5. Model validation for the period of the data

For initial model validation, the estimated STM-E model is used to generate distributions of the N -year maximum H_S per location corresponding to period $N = 21$ years of the original Todai WW3 hindcast via Equation (4). Then the actual observed maximum per location in the 21 period is isolated from the hindcast. Finally, again using Equation (4), the p -value corresponding to the actual maximum per location under the model for the estimated 21-year maximum is estimated, and shown in Figure 10. Locations with $p \leq 0.025$ or $p > 0.975$ are unusual, and their number corresponds approximately to 5% of the number n_R of locations. Since the observed maxima are spatially-correlated, it is not surprising that p -value varies smoothly spatially, and that all locations in some small neighbourhoods exceed the 5%. Note red contour lines near coasts and model boundary at the $p=0.025$ level, since values of H_S there are small and zero at boundary.

[Figure 10 about here.]

4.6. Spatial variability in distribution of exposure

For the five locations P1-P5 identified in Figure 8, a bootstrap analysis was performed to evaluate the uncertainty in the empirical distribution of exposure E_j per location. Figure 11 shows

bootstrap \pm one standard deviation uncertainty bands for the distribution of E_j . It is clear from the figure that there are systematic differences between the distributions, as would be expected since exposure is responsible ultimately for spatial differences in return value estimates. In particular, the distribution at P5 and P3, corresponding to the most easterly locations appear quite different to the others, with greater proportions of small values of exposure. This reflects the decrease of track density in the eastern region, as seen in Figure 2. In addition, the strength of tropical cyclones generally weakens as they move north. As a result, locations P3 and P5 have low exposure to cyclones.

[Figure 11 about here.]

We also examine the relative contributions of variability in STM and exposure at the five locations P1-P5. We perform a bootstrap reampling analysis on the full STM-E model, and estimate bootstrap uncertainty distributions for the 100-year return value of H_S at each of P1-P5. We also estimate the corresponding bootstrap uncertainty distribution when only the exposure data is resampled; this allows us to quantify (in metres) the effect of exposure variability on return value estimates. Table 1 given interquartile ranges for bootstrap uncertainty from the full STM-E model, and from only the exposure model. We see that bootstrap uncertainty of full STM-E reflects the spatial variation of the 100-year return value (see Figure 8). In contrast, the variability in exposure contributes between 0.8m and 1.0m at all locations.

[Table 1 about here.]

5. Testing modelling assumptions

The success of the current approach relies critically on our ability to show that simplifying assumptions regarding the characteristics of STM and exposure are justified for the data to hand. In particular, the approach assumes that (a) the distribution F_S of STM does not depend on cyclone track, environmental covariates, space and time, and (b) the distribution of exposure per location does not depend on STM, cyclone track, environmental covariates and time. In this section, we outline a number of statistical diagnostic tests undertaken to examine the plausibility of our modelling assumptions, and hence the credibility of return value estimates in particular.

In estimating the STM-E model in Section 4, we also make a number of arbitrary choices of parameter setting for e.g. specification of spatial domain \mathcal{R} , isolation of storm peak events per location. We report briefly a sensitivity study into some of these more arbitrary parameter settings.

5.1. No spatial trend in STM

First we examine the possibility of a spatial trend in the set $\{s_i\}$ of STM values representing random variable S . To achieve this, we use the set $\{s_i\}$ of STM magnitudes and the longitude-latitude locations $\{\mathbf{x}_i\}$ of STMs. Then we estimate the linear correlation between S with distance ℓ along a straight line with arbitrary orientation θ (and direction vector $\mathbf{d} = (\cos(\theta), \sin(\theta))$ in longitude and latitude space), retaining the maximum slope c_0 found, using

$$c_0 = \max_{\theta \in [0, 2\pi)} \text{corr} [\{s_i\}, \{\mathbf{x}_i \cdot \mathbf{d}\}] \quad (6)$$

where $\mathbf{x}_i \cdot \mathbf{d}$ represents the scalar product of \mathbf{x}_i and \mathbf{d} within the spatial domain considered. Note that the value of c_0 must be non-negative, since we could always add π to θ in the case that c_0 was negative, to change its sign. Next we estimate the probability density $f_{C;R}$ of the randomized permutation distribution of maximum correlation by repeating the estimation for $n_P = 1000$ random permutations of the form $\{s_{Q(i)}\}$, where Q represents a random permutation of $1, 2, \dots, n_S$. We use the resulting sample $\{c_k\}_{k=1}^{n_P}$ as a direct empirical estimate of the density $f_{C;R}$. Then we compare c_0 with its randomised permutation distribution. If c_0 corresponded to an unusual correlation, it would be extreme in the right hand tail of the randomised permutation distribution. Inspection of Figure 12 shows that this is not the case. As required, validation procedures can be enhanced to investigate other potential dependencies, e.g. the approach of [19].

[Figure 12 about here.]

5.2. Exposure independent of STM

We would also like to demonstrate that exposure E_j at location j does not depend on the value S of STM, since otherwise we could not justify the simple method for estimating E_j in Section 3. To achieve this we estimate Kendall's tau statistic for the rank correlation between E_j and S at each location. Specifically, per location j we consider the set $\{s_i\}$ of STM magnitudes and the set $\{e_{ij}\}_{i=1}^{n_S}$ of exposure values, and estimate Kendall's tau τ_j statistic using

$$\tau_j = \frac{1}{n_S(n_S-1)} \sum_{i \neq k} \text{sgn}(s_i - s_k) \text{sgn}(e_{ij} - e_{kj}). \quad (7)$$

If the values of S and E_j increase together, the value of τ will be near to unity. If there is no particular relationship between S and E_j , the value of τ will be near zero. For large n_S , if S and E_j are actually independent, the value of τ is approximately Gaussian-distributed with zero mean and variance $2(2n_S + 5)/(9n_S(n_S - 1))$. This provides a means of identifying unusual values of τ which may indicate dependence between S and E_j . Figure 13 shows the value of τ for all spatial locations. For the majority of the domain, the relationship between S and E_j does not appear to be inconsistent with the assumption of independence. At the 90% level, approximately 10% of the geographical area is expected to yield values above the 90% value of Kendall tau, due to random variation. In addition, it is not surprising, due to the spatial correlation of STM and E_j , that high values of Kendall tau occur in clusters of neighbouring locations. Most of the large values of significant wave height at near-shore locations are below the threshold for STM-E modelling, set by us to 3m for this work. Thus, exposure for these areas is mostly zero and these areas therefore fail the Kendall tau test. We consider this issue of secondary concern in the current work, since the wave hindcast model resolution is not high enough anyway to resolve the characteristics of these areas well. This problem of course could be alleviated by using higher resolution wave model output (e.g. at 1 km) and setting low STM-E thresholds for such regions.

[Figure 13 about here.]

5.3. Sensitivity to peak-picking parameters

Several model set-up parameters have been chosen based on experience by the authors, but it is nevertheless critically important to confirm that varying these parameters does not materially change inferences for return values in particular. Specifically, we assume the peak-picking procedure isolates independent storm peak events using a combination of two parameters: peak-picking threshold and peak merge interval (e.g. [18]). Peak-picking threshold for isolation of H_S per location was set at 3m, and peak merge interval for merging peaks occurring close together in time was set at 1.5 days. Figure 23 and Figure 24 in the Appendix provide illustrative results analogous to Figure 8 from a sensitivity study into choices of peak-picking threshold and merge interval. From various diagnostics plots generated during the course of the analysis, we choose here the return period value itself to illustrate the overall distribution. Figure 8, Figure 23 and Figure 24 show small differences compared to one another, but larger-scale features are well preserved. Our conclusion

from the sensitivity study was that estimates for return values are not overly influenced by the choices made.

5.4. Sensitivity to choice of spatial region

Choice of spatial domain is another modelling choice made on the basis of elementary physical considerations. Yet region choice is critical to the success of the STM-E model for two reasons in particular. Firstly, we assume that the extremal behaviour of STM can be considered homogeneous in the region. This suggests that the region should not be too large so that the same physics is active throughout it. The diagnostics presented in Section 5, and Section 5.1 and 5.2 in particular, appear to justify this assumption for the spatial domain selected.

A second assumption is that the region contains sufficient evidence for cyclone events and their characteristics to allow reasonable estimation of tails of distributions for H_S per location. This suggests that the region selected should not be too small. Here we consider the effect of reducing the spatial domain on estimation of return values. Specifically, we choose two additional regions, corresponding to subsets of the original spatial domain, and repeat the whole analysis procedure independently for the new regions. New regions are labelled B and C for convenience. Relative to the original domain (labelled A), region B is restricted in latitude only. Region C is severely restricted in longitude and latitude. Resulting spatial maps of the 100-year return value are shown in Figures 14 and Figure 15.

[Figure 14 about here.]

[Figure 15 about here.]

[Figure 16 about here.]

Return value estimates for H_S using region B appear consistent with those obtained using the original spatial domain. However, return value estimates using region C alone are much smaller. This is easily explained: in the analysis based on region C alone excludes the largest cyclone event observed on the full spatial domain. Clearly, the region for analysis must be chosen carefully. It is interesting to confirm whether the result based on region C along is actually inconsistent with the result using the whole domain A. To achieve this, we use a bootstrap analysis to estimate a 95% uncertainty band per location for the 100-year return value of H_S using the full spatial

domain. In Figure 16, we show the 2.5 percentile of that bootstrap distribution for region C only. We see that the values in Figure 15 are everywhere larger than those in Figure 16, suggesting general consistency. Of course, especially when the sample size for analysis is small, extreme value estimation is particularly sensitive to individual large values in the sample.

STM is the maximum significant wave height for the period of a typhoon within the region considered (A, B or C), and since some typhoon tracks are not completely contained within the region in general, the STM sometimes occurs outside the region. For small regions, this produces underestimation of storm severity. However, this effect reduces as the size of the region increases, as can be seen from comparison of results for regions A and B, as opposed to results for regions B and C.

The choice of optimal spatial region for any given analysis involves a classic bias-variance trade-off. In choosing a small region, we can be confident that tropical cyclones included are representative of that region, but the number of tropical cyclones available for analysis will be small; hence uncertainties in return values will be large. As we increase region size, then the tropical cyclones in general become less representative of any specific point within the region, but their number increases and hence uncertainty in return values reduces. For some intermediate region size, there will be an optimal compromise between bias and uncertainty. Similarly, region shape could be optimised. This would be an interesting topic for further study.

5.5. *Effect of truncating exposure*

It might be expected that the largest contributions to 100-year return values for H_S at location r_j would correspond to relatively large values of exposure E_j there, and that the low tail of the distribution of exposure would be of little importance in the estimation of return values corresponding to long return periods. We test this idea at the five locations identified in Figure 8, by setting the distribution $F_{E_j}(e) = 0$ for values of exposure less than some $\theta \in [0, 1]$. The effect of this truncation is to neglect contributions of small exposure to return value estimates. From the results shown in Figure 17, the 100-year return value for H_S does not change for $\theta \leq 0.3$. But for larger values of θ , the return value at each of P1-P5 gradually decreases, clearly indicating the importance of middle-ranging exposure for return value estimation for this particular application.

[Figure 17 about here.]

We infer that STM-E provides a good model for estimation of the 100-year return value for Hs spatially. Specifically, the modelling assumptions underlying STM-E are satisfied for the present cyclone analysis; inferences using the STM-E model are consistent with the cyclone data; and, estimates for the 100-year Hs are considerably less uncertain per location than those obtained using a single-site analysis. In this sense, the STM-E model is more parsimonious than single location analysis, since it can explain the observed data without recourse to high spatial variability in extreme value parameters, return values and their uncertainties. Moreover, the smooth spatial variation of 100-year Hs, and its uncertainty, from STM-E appears more consistent with physical intuition than that suggested by a single point analysis.

6. Comparison with single location analysis

It is also interesting to compare estimates for the 100-year return value from the STM-E model with those from conventional location-by-location analysis. To this end, the estimate for the 100-year return value was found independently for each location j using the set of $\{h_{ij}\}_{i=1}^{n_S}$ values isolated in Section 3, as shown in Figure 18; in other words, the analysis was conducted independently location-by-location, for all of approximately 38,000 locations. Figure 19 gives the bias between estimates from this “single point” and STM-E models. There is clear spatial dependence in the bias, suggesting that single point estimation is strongly conditioned by proximity of large cyclone tracks (see Figure 1).

[Figure 18 about here.]

[Figure 19 about here.]

Single location analysis of course also produces much higher variability in N -year maxima. Figure 20 and Figure 21 show estimates for the interquartile range of the distribution of the 100-year maximum event using the single point and proposed spatial model. A comparison of empirical densities for interquartile range from single point and STM-E analyses is given in Figure 22. Uncertainties from single point analysis vary spatially in a similar manner to the bias shown in Figure 19, whereas uncertainties from STM-E are clearly spatially less variable.

[Figure 20 about here.]

[Figure 21 about here.]

[Figure 22 about here.]

7. Conclusion

We estimate a model (STM-E) for the spatial characteristics of storm peak significant wave height in a tropical cyclone, and validate its performance using diagnostic tests. The model has two components: *space-time maximum* STM, which characterises the distribution of the maximum H_S (over space and time) in a cyclone and *exposure*, which quantifies the maximum H_S observed at a location for a given cyclone event, expressed as a fraction of the STM for the cyclone. We show that the modelling assumptions underlying STM-E appear to be satisfied at least approximately for the current application, and conduct a number of sensitivity studies to ensure stable behaviour of the model. Using STM-E, we estimate spatial maps of the 100-year return value for H_S in the North West Pacific. Since exposure quantifies spatial dependence on an absolute spatial grid, the effects of coastlines and islands on return values are easily incorporated. Compared with estimation using data from a single location, STM-E provides large reductions in the variability of return value estimates. For cyclone-dominated regions like the North West Pacific, when the sample for estimation of metocean design criteria is small, we believe the proposed model is a useful addition to the metocean engineer's toolkit.

Acknowledgements

This work was supported by JSPS KAKENHI Grant Number JP15K18290.

References

- [1] S. J. Buchan, P. G. Black, R. L. Cohen, The impact of tropical cyclone Olivia on Australia's Northwest Shelf., Offshore Technology Conference, Houston, OTC-10791.
- [2] P. Jonathan, K. C. Ewans, Statistical modelling of extreme ocean environments with implications for marine design : a review, Ocean Eng. 62 (2013) 91–109.
- [3] R. Wada, T. Waseda, Benchmark for sources of uncertainty in extreme wave analysis, Proc. 37rd Conf. Offshore Mech. Arct. Eng. (Accepted 2018).

- [4] I. R. Young, Parametric hurricane wave prediction model, *Journal of Waterway, Port, Coastal, and Ocean Engineering* 114 (5) (1988) 637–652.
- [5] J. C. Heideman, D. A. Mitchell, Grid point pooling in extreme value analysis of hurricane hindcast data, *J. Waterway, Port, Coastal, Ocean Eng.* 135 (2009) 31–38.
- [6] P. Vickery, D. Wadhera, J. Stear, A synthetic model for Gulf of Mexico hurricanes, *Offshore Technology Conference, Houston, OTC-20699*.
- [7] P. J. Vickery, P. F. Skerlj, L. A. Twisdale, Simulation of hurricane risk in the U.S. using empirical track model, *J. Struct. Eng.* 126 (2000) 1222–1237.
- [8] A. C. Davison, S. A. Padoan, M. Ribatet, Statistical modelling of spatial extremes, *Statist. Sci.* 27 (2012) 161–186.
- [9] E. Ross, M. Kereszturi, M. van Nee, D. Randell, P. Jonathan, On the spatial dependence of extreme ocean storm seas, *Ocean Eng.* 145 (2017) 1–14.
- [10] H. Takagi, W. Wu, Maximum wind radius estimated by the 50 kt radius: improvement of storm surge forecasting over the western North Pacific, *Nat. Hazards Earth Sys.* 16 (2016) 705–717.
- [11] I. R. Young, *Wind generated ocean waves*, Vol. 2, Elsevier, 1999.
- [12] A. Webb, T. Waseda, W. Fujimoto, K. Horiuchi, K. Kiyomatsu, K. Matsuda, Y. Miyazawa, S. Varlamov, J. Yoshikawa, A high-resolution wave and current resource assessment of Japan: the Web GIS dataset, *arXiv preprint arXiv:1607.02251*.
- [13] D. P. Dee, S. M. Uppala, A. J. Simmons, P. Berrisford, P. Poli, S. Kobayashi, U. Andrae, M. A. Balmaseda, G. Balsamo, P. Bauer, et al., The ERA-Interim reanalysis: Configuration and performance of the data assimilation system, *Q. J. Roy. Meteorol. Soc.* 137 (2011) 553–597.
- [14] J. E. Stopa, K. F. Cheung, Intercomparison of wind and wave data from the ECMWF Reanalysis Interim and the NCEP Climate Forecast System Reanalysis, *Ocean Model.* 75 (2014) 65–83.
- [15] K. R. Knapp, M. C. Kruk, D. H. Levinson, H. J. Diamond, C. J. Neumann, The international best track archive for climate stewardship (IBTrACS) unifying tropical cyclone data, *Bull. Am. Meteorol. Soc.* 91 (2010) 363–376.

- [16] R. Wada, T. Waseda, P. Jonathan, Extreme value estimation using the likelihood-weighted method, *Ocean Eng.* 124 (2016) 241–251.
- [17] E. Ross, D. Randell, K. Ewans, G. Feld, P. Jonathan, Efficient estimation of return value distributions from non-stationary marginal extreme value models using Bayesian inference, *Ocean Eng.* 142 (2017) 315–328.
- [18] K. C. Ewans, P. Jonathan, The effect of directionality on northern North Sea extreme wave design criteria, *J. Offshore. Arct. Eng.* 130 (2008) 041604:1–041604:8.
- [19] T. M. Hall, S. Jewson, Statistical modelling of north atlantic tropical cyclone tracks, *Tellus A: Dynamic Meteorology and Oceanography* 59 (4) (2007) 486–498.

Appendix A. Investigation of effect of storm peak-picking threshold

This section provides figures supporting the discussion on storm peak-picking threshold in Section 5.3.

[Figure 23 about here.]

[Figure 24 about here.]

List of Figures

1	Maximum value of H_S per location in 21 years of Todai WW3 hindcast corresponding to tropical cyclones. Red contour lines enclose neighbourhoods with $H_S > 15.5\text{m}$. The Japanese mainland is shown in grey.	23
2	Tracks of 63 tropical cyclone centres in the period [1994,2014] from IBTrACS.	24
3	Contour plot of spatial distribution of storm peak H_S for an illustrative tropical cyclone from September 1996. The location of the cyclone STM is shown with an asterix.	25
4	Location of STM for each tropical cyclone. Circle radius scales linearly with STM magnitude from approximately 10m to approximately 21m.	26
5	Extreme value estimation for STM from Todai WW3 hindcast using the likelihood weighted method. Left hand panel shows empirical and posterior predictive tails. The right hand panel shows the posterior distribution of generalised Pareto shape ξ and scale σ	27
6	Contour plots of exposure E for six illustrative tropical cyclone (TC) events, with tropical cyclone track in red. Tropical cyclone indicator and corresponding value of STM for each cyclone (ST) given in panel titles.	28
7	Solid lines show cumulative distribution functions of H_S for a single storm peak event at location P2 (blue, see Figure 8) or a single STM event (orange). Dashed lines show the corresponding distributions for the 100-year maximum event at P2, and the 100-year maximum STM.	29
8	Spatial map of 100-year return value for H_S . Also shown are 5 locations Point#1-Point#5 (P1-P5 for brevity in the text) used in this section, and in Section 5 and Section 6.	30
9	Focussed spatial view of 100-year H_S return value estimates, emphasising their behaviour around coastlines and islands.	31
10	p -values for actual observed maximum H_S per location under the estimated distribution. Regions enclosed by red contours indicate $p \leq 0.025$. Nowhere is $p > 0.975$. The area enclosed by red contours corresponds to 1.8% of the total.	32
11	Estimates for distributions of exposure for locations P1-P5. Thin lines indicate \pm one standard deviation.	33
12	Randomised permutation test for the correlation of STM values along any straight line in longitude-latitude space. The randomised permutation density for correlation (blue) is compared with the correlation (equal to 0.00007) observed for the actual sample (red).	34
13	Kendall's tau statistic evaluated for all spatial locations. Red contour encompassed neighbourhoods within which the value of Kendall's tau is unusually large indicating possible dependence between S and E_j	35
14	Spatial map of 100-year return value for H_S for medium-sized region B, to be compared with Figure 8.	36
15	Spatial map of 100-year return value for H_S for small region C, to be compared with Figure 8.	37
16	2.5%ile of bootstrap uncertainty distribution based on bootstrap analysis of full spatial domain A, focussed on region C for comparison with Figure 15.	38

17 Effect of truncation of distribution of exposure E at probability level θ for each of the five locations P1-P5. 39

18 100-year return value estimates for H_S per location estimated from single point analysis. 40

19 Difference between 100-year return value estimates for H_S per location estimate from single point analysis, and that estimated using the STM-E spatial model. 41

20 Interquartile range from distribution of the 100-year maximum event from single point analysis. Note, for ease of comparison with Figure 21, that values of interquartile range exceeding 10m are truncated at 10m here. The full distribution of interquartile range is shown in Figure 22. 42

21 Interquartile range from distribution of the 100-year maximum event from STM-E spatial model, using same colour scale as Figure 20. 43

22 Empirical densities for the interquartile range of the distribution of the 100-year maximum event from single point and STM-E estimates illustrated spatially in Figure 20 and Figure 21. 44

23 Spatial map of 100-year return value for H_S using 5m peak-picking threshold, to be compared with Figure 8. 45

24 Spatial map of 100-year return value for H_S using 3 day peak merge interval, to be compared with Figure 8. 46

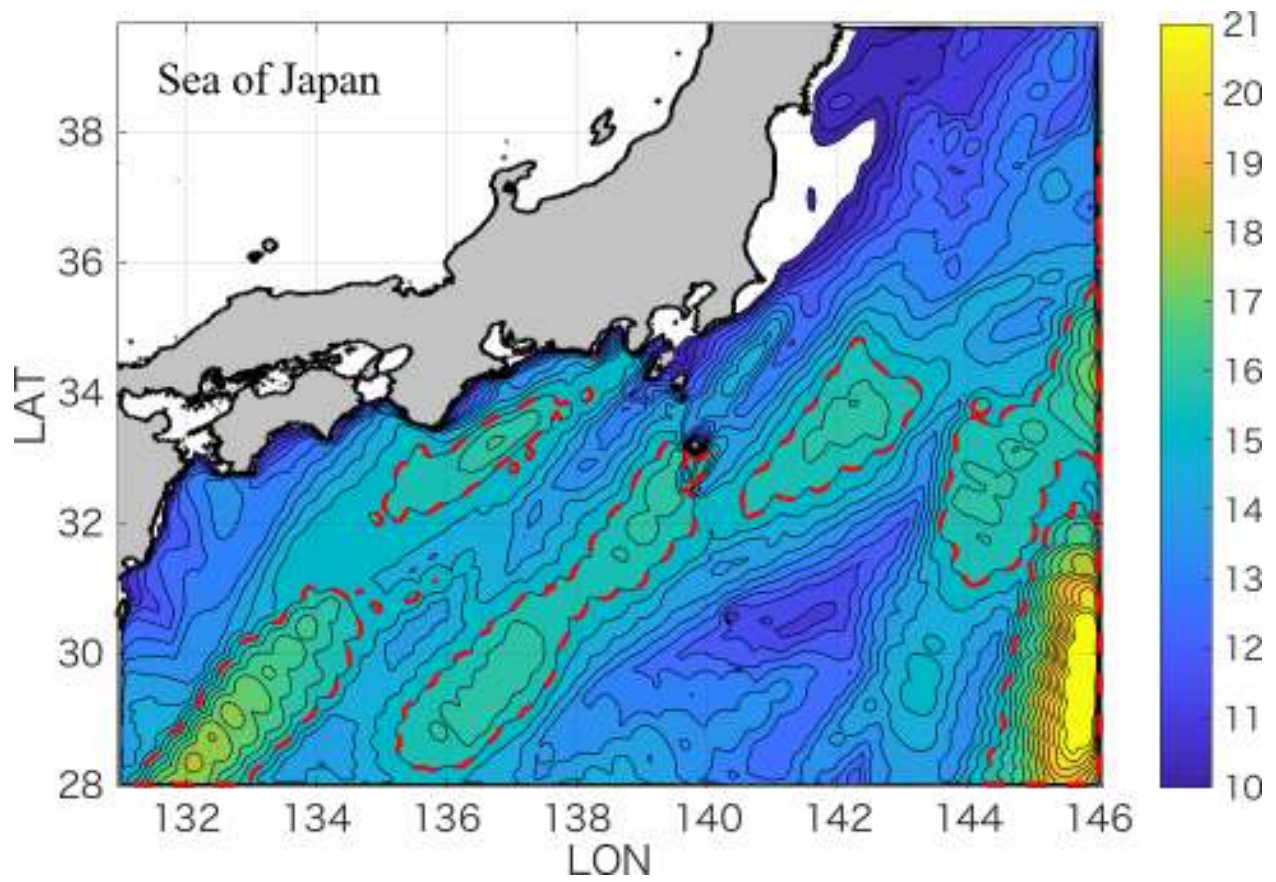


Figure 1: Maximum value of H_S per location in 21 years of Todai WW3 hindcast corresponding to tropical cyclones. Red contour lines enclose neighbourhoods with $H_S > 15.5$ m. The Japanese mainland is shown in grey.

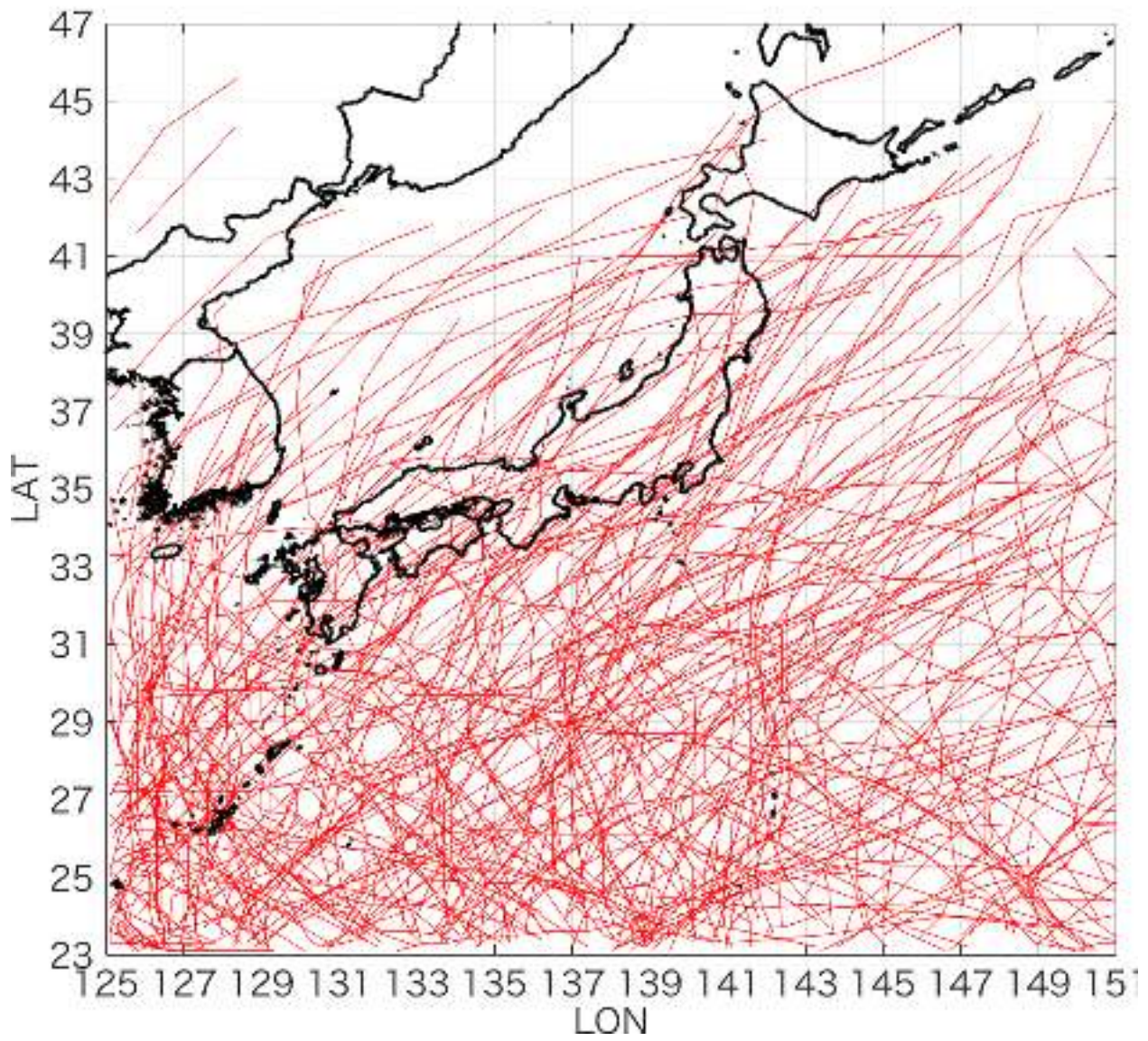


Figure 2: Tracks of 63 tropical cyclone centres in the period [1994,2014] from IBTrACS.

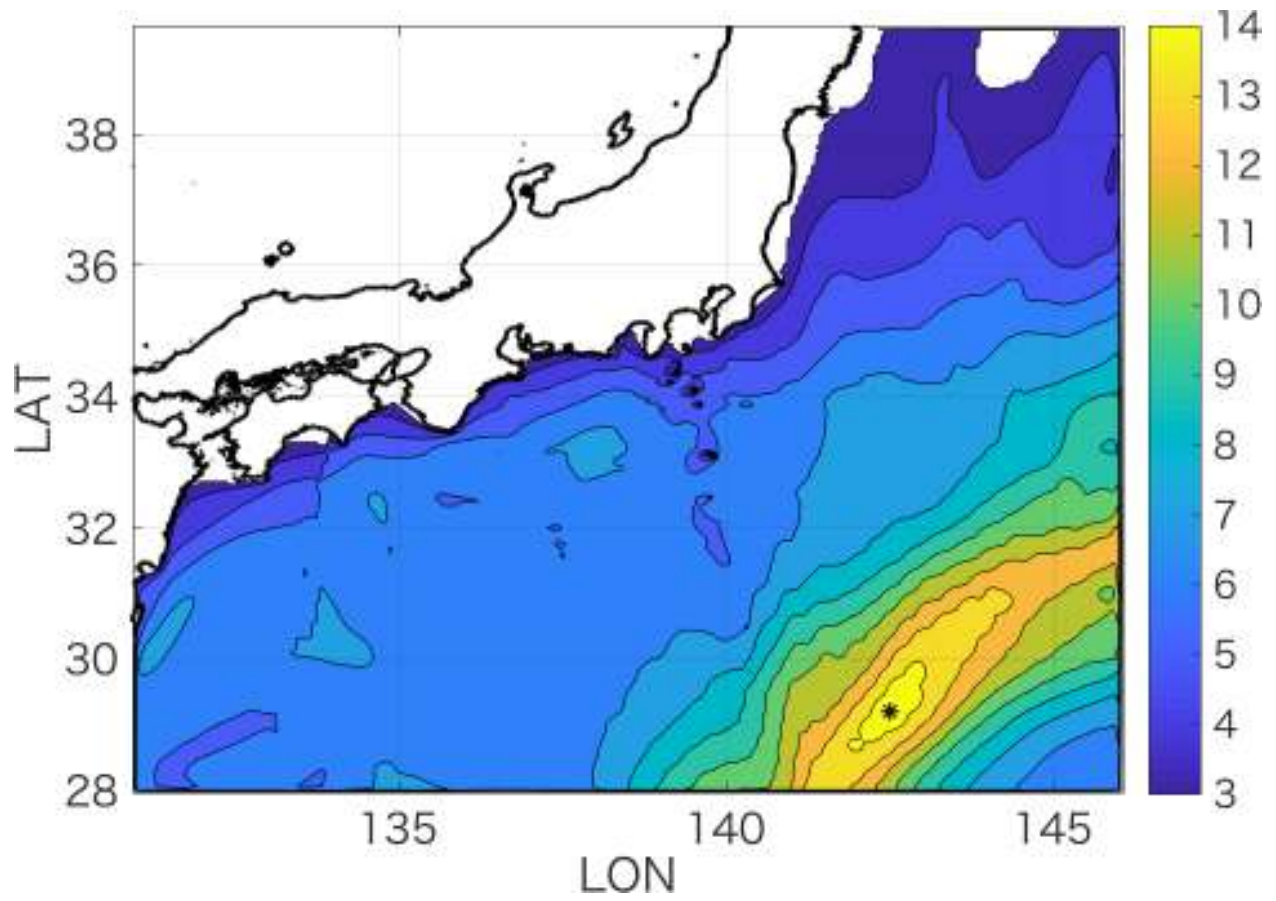


Figure 3: Contour plot of spatial distribution of storm peak H_S for an illustrative tropical cyclone from September 1996. The location of the cyclone STM is shown with an asterisk.

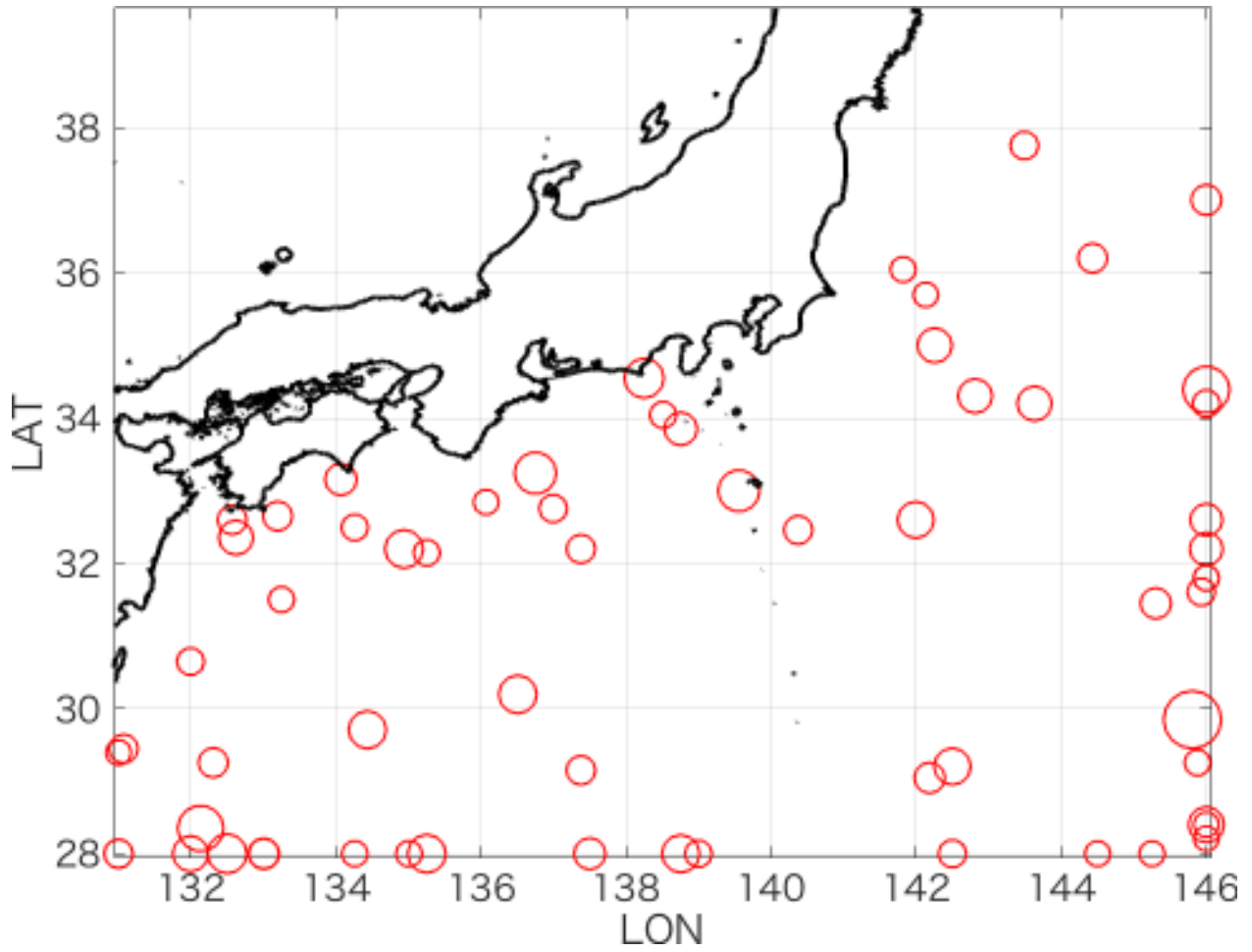


Figure 4: Location of STM for each tropical cyclone. Circle radius scales linearly with STM magnitude from approximately 10m to approximately 21m.

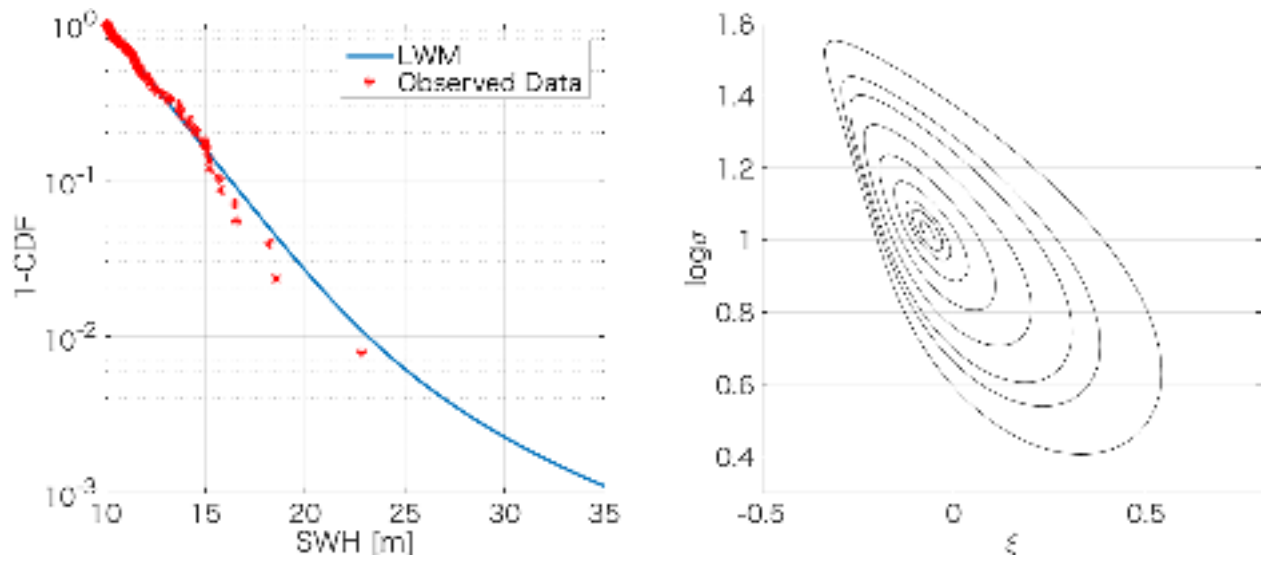


Figure 5: Extreme value estimation for STM from Todai WW3 hindcast using the likelihood weighted method. Left hand panel shows empirical and posterior predictive tails. The right hand panel shows the posterior distribution of generalised Pareto shape ξ and scale σ .

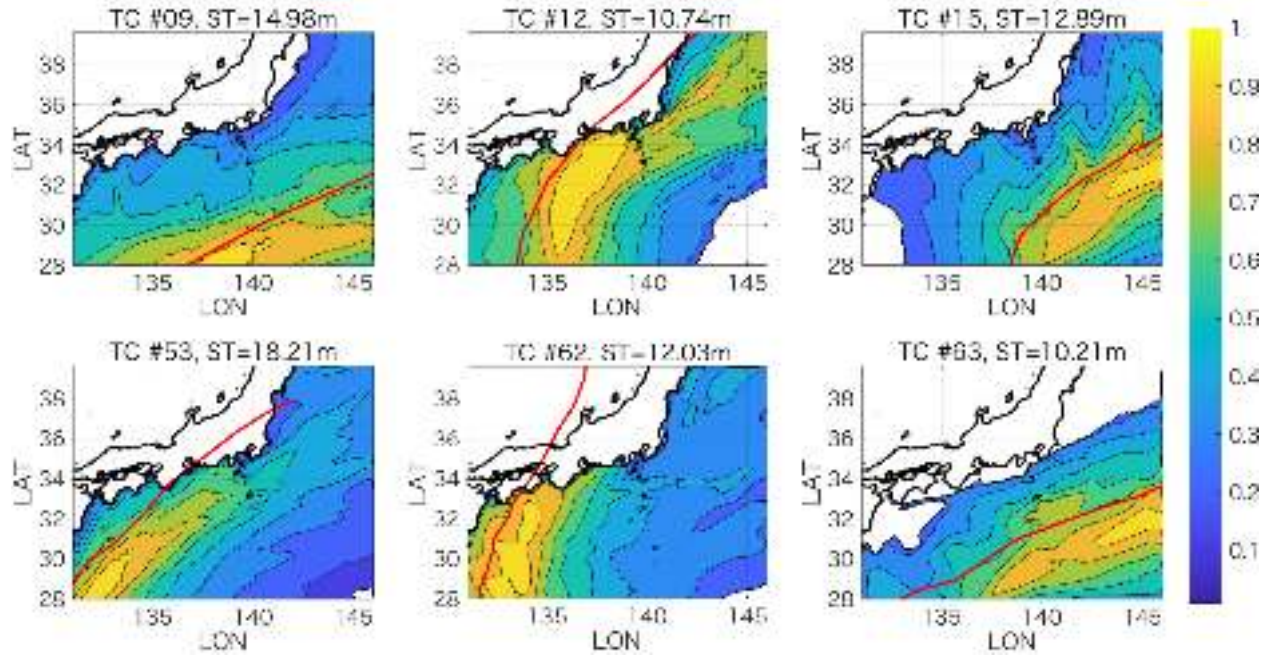


Figure 6: Contour plots of exposure E for six illustrative tropical cyclone (TC) events, with tropical cyclone track in red. Tropical cyclone indicator and corresponding value of STM for each cyclone (ST) given in panel titles.

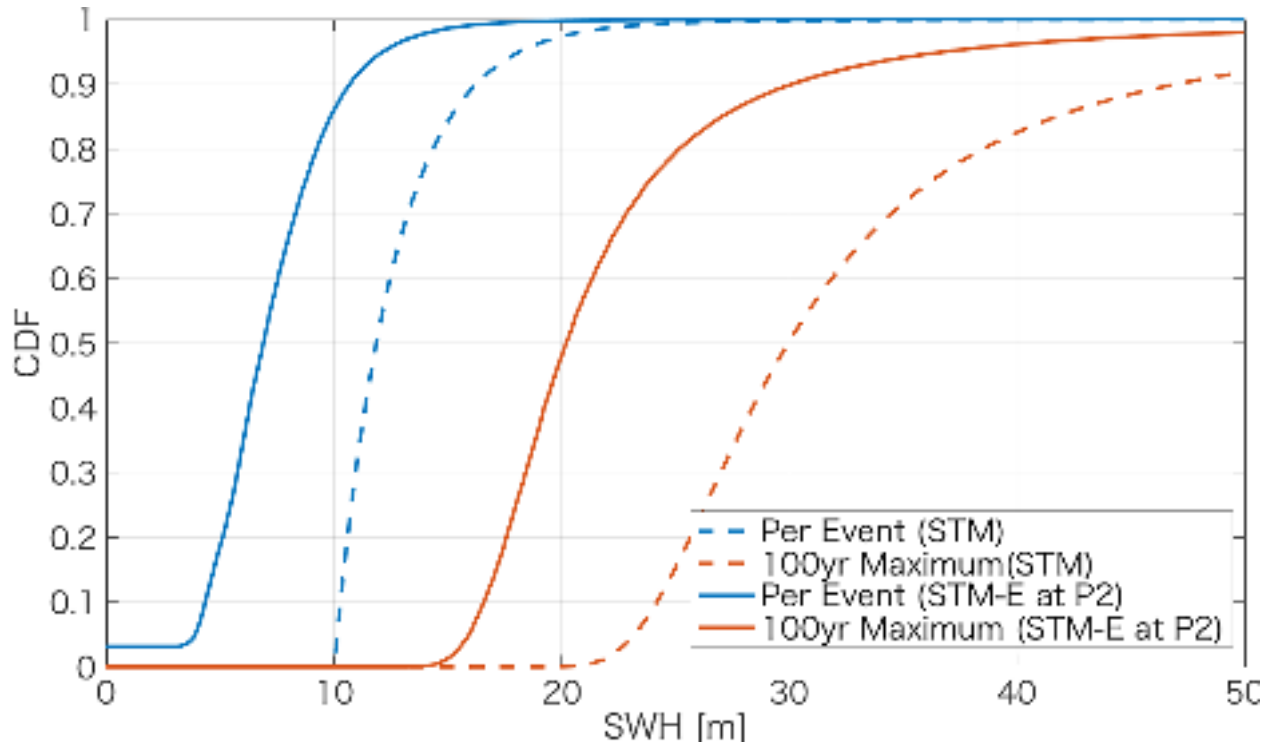


Figure 7: Solid lines show cumulative distribution functions of H_S for a single storm peak event at location P2 (blue, see Figure 8) or a single STM event (orange). Dashed lines show the corresponding distributions for the 100-year maximum event at P2, and the 100-year maximum STM.

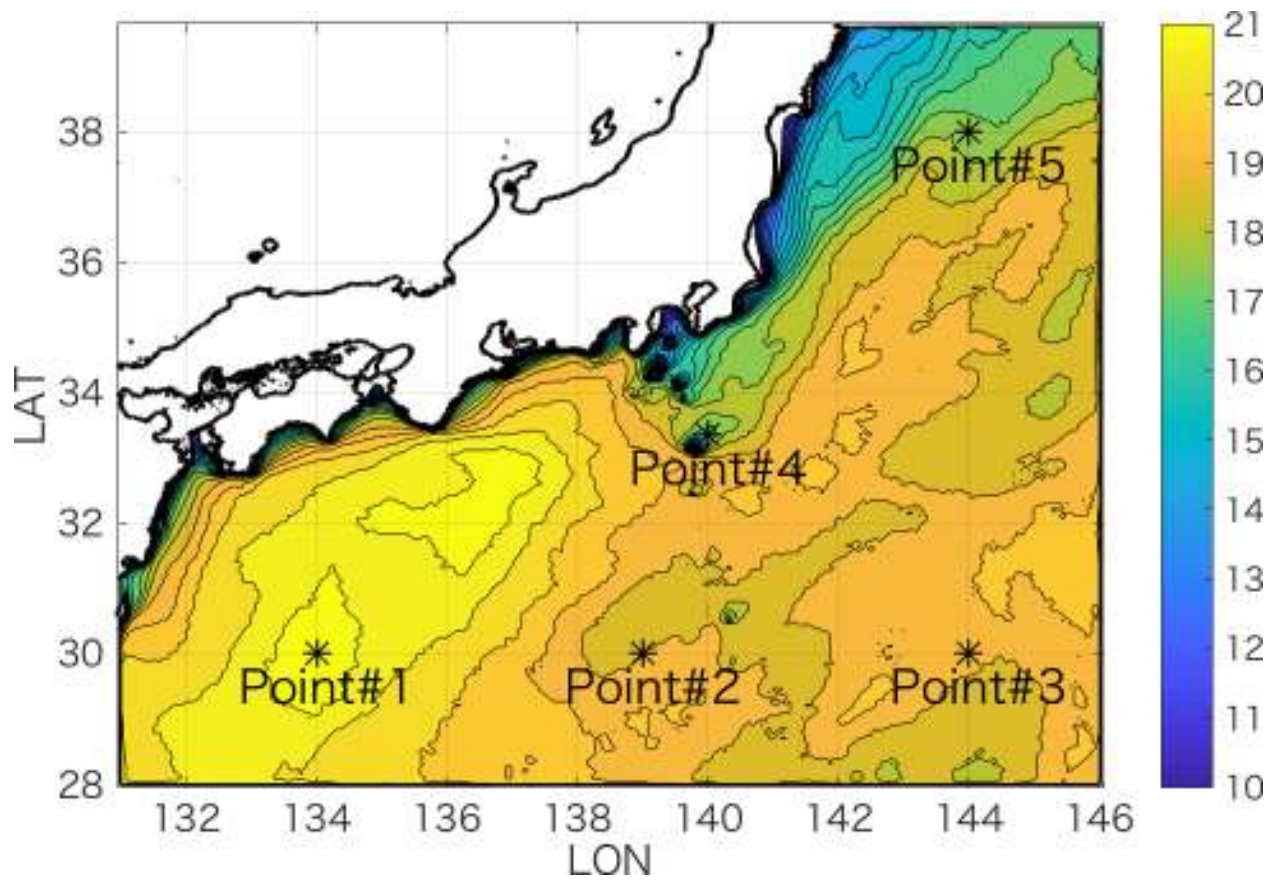


Figure 8: Spatial map of 100-year return value for H_s . Also shown are 5 locations Point#1-Point#5 (P1-P5 for brevity in the text) used in this section, and in Section 5 and Section 6.

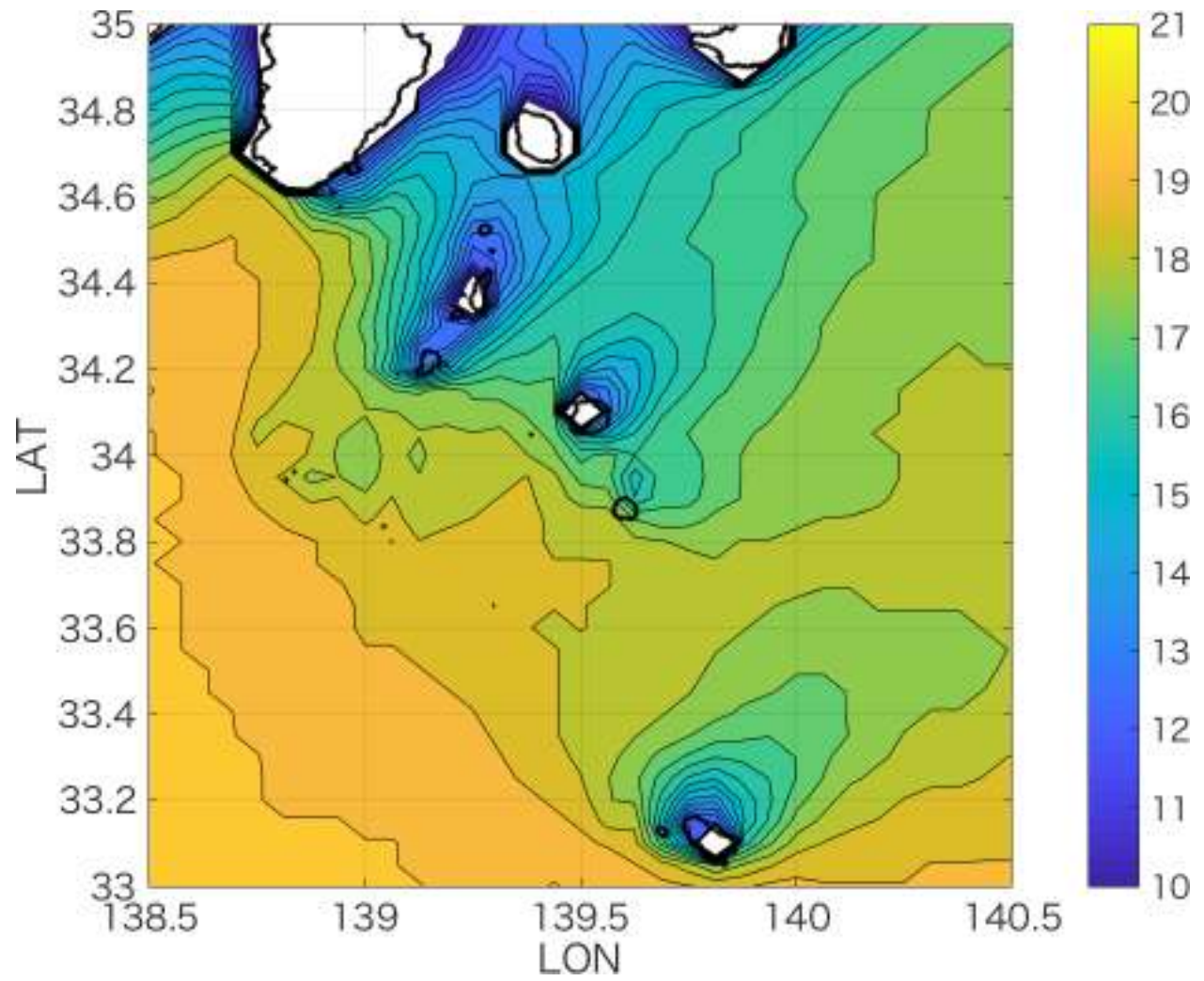


Figure 9: Focussed spatial view of 100-year H_S return value estimates, emphasising their behaviour around coastlines and islands.

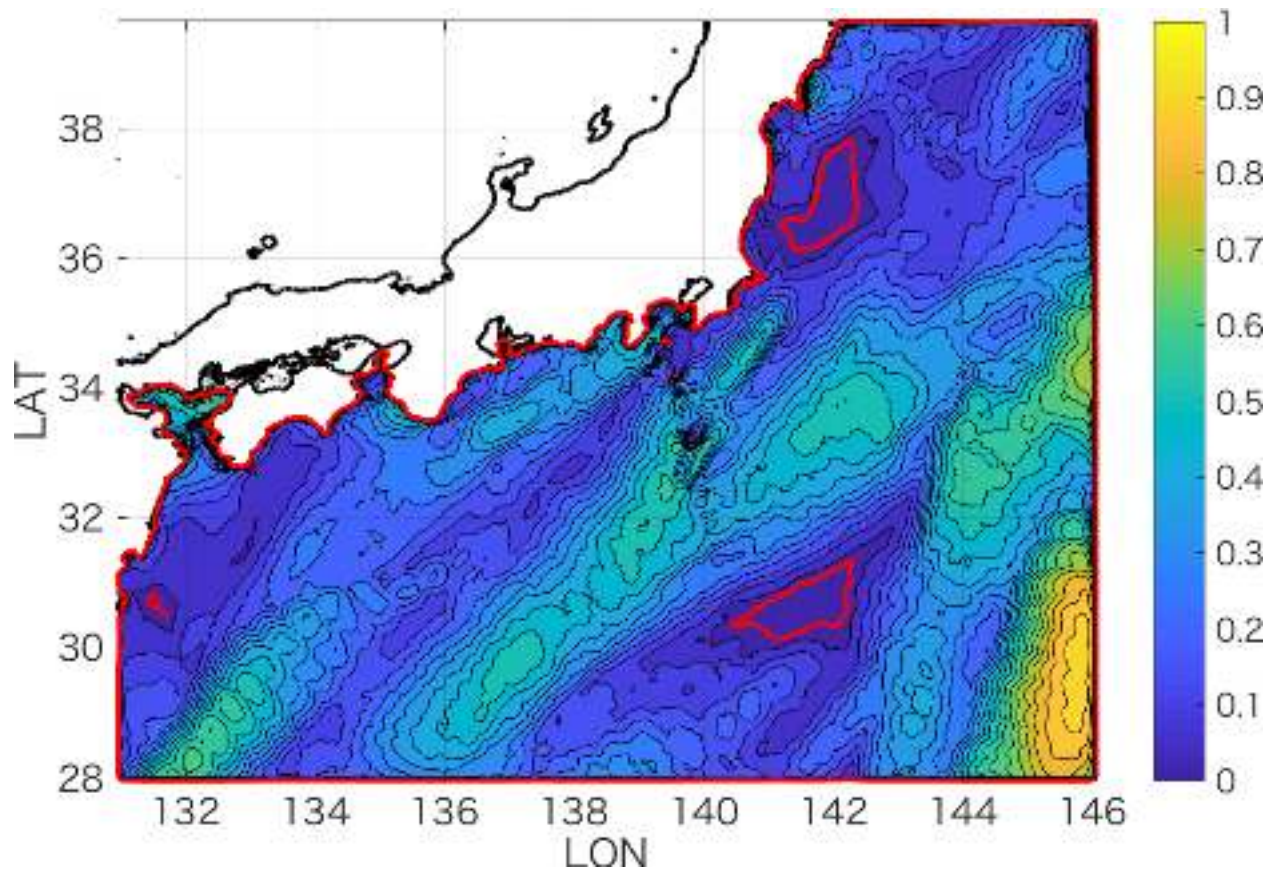


Figure 10: p -values for actual observed maximum H_s per location under the estimated distribution. Regions enclosed by red contours indicate $p \leq 0.025$. Nowhere is $p > 0.975$. The area enclosed by red contours corresponds to 1.8% of the total.

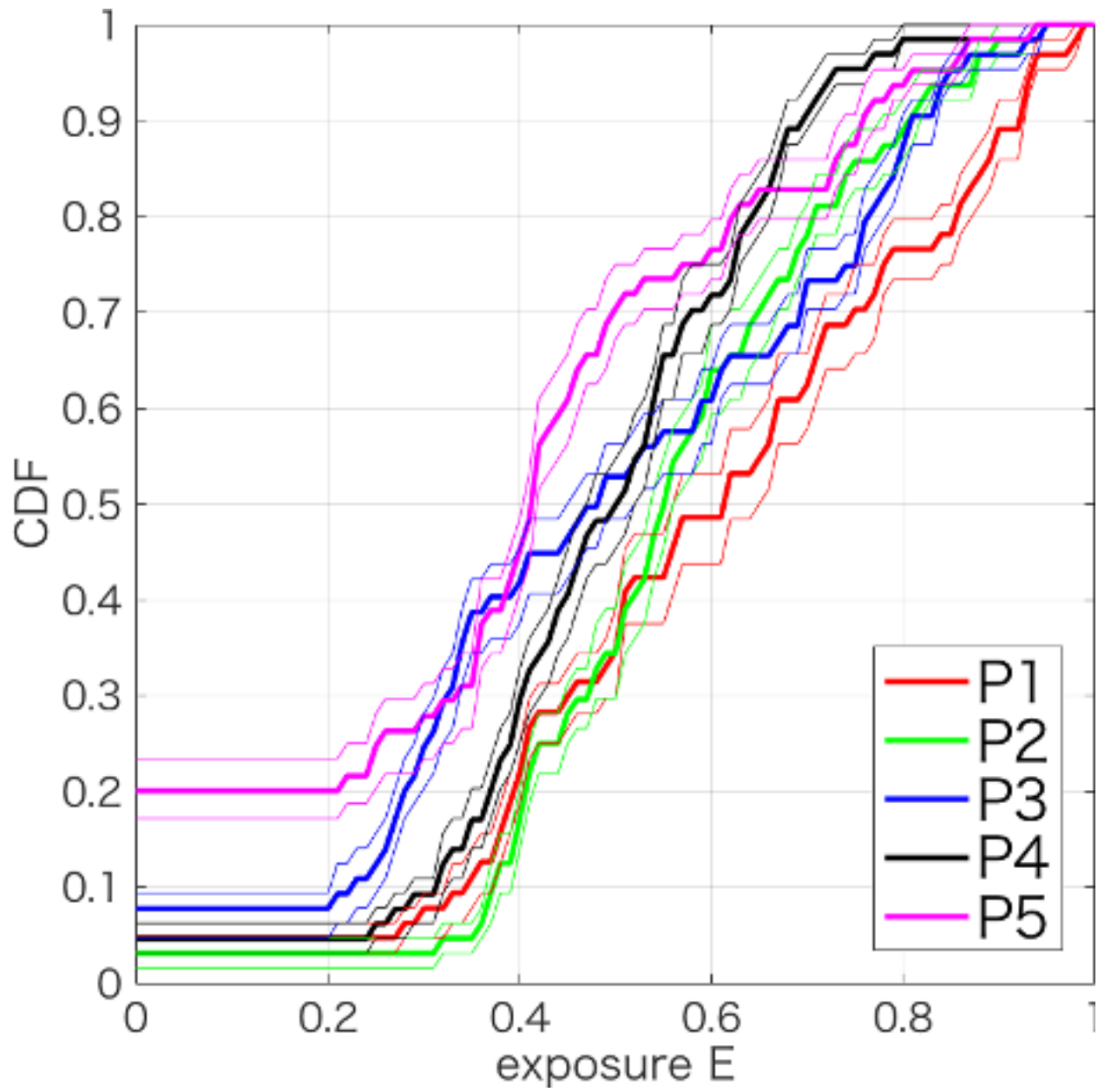


Figure 11: Estimates for distributions of exposure for locations P1-P5. Thin lines indicate \pm one standard deviation.

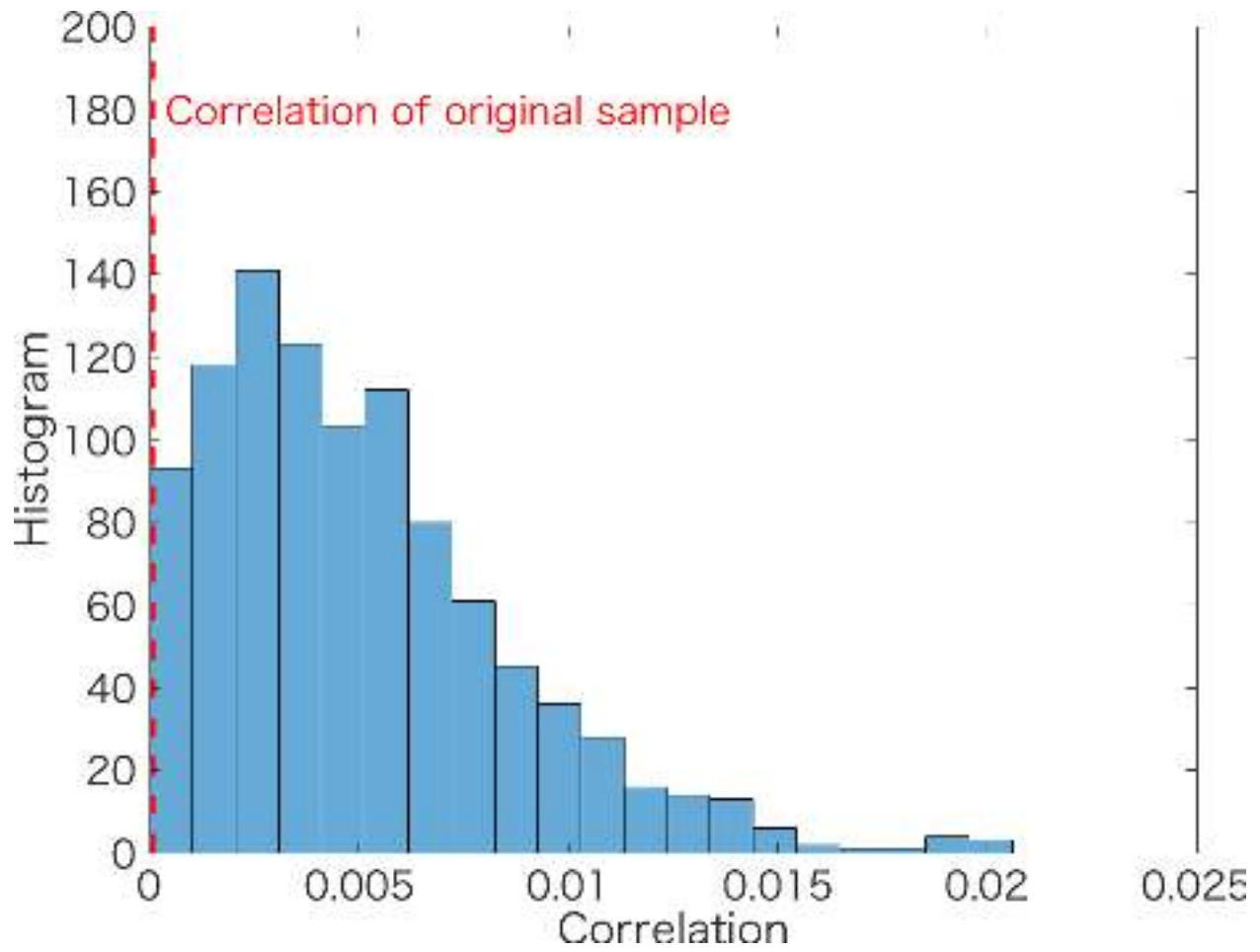


Figure 12: Randomised permutation test for the correlation of STM values along any straight line in longitude-latitude space. The randomised permutation density for correlation (blue) is compared with the correlation (equal to 0.00007) observed for the actual sample (red).

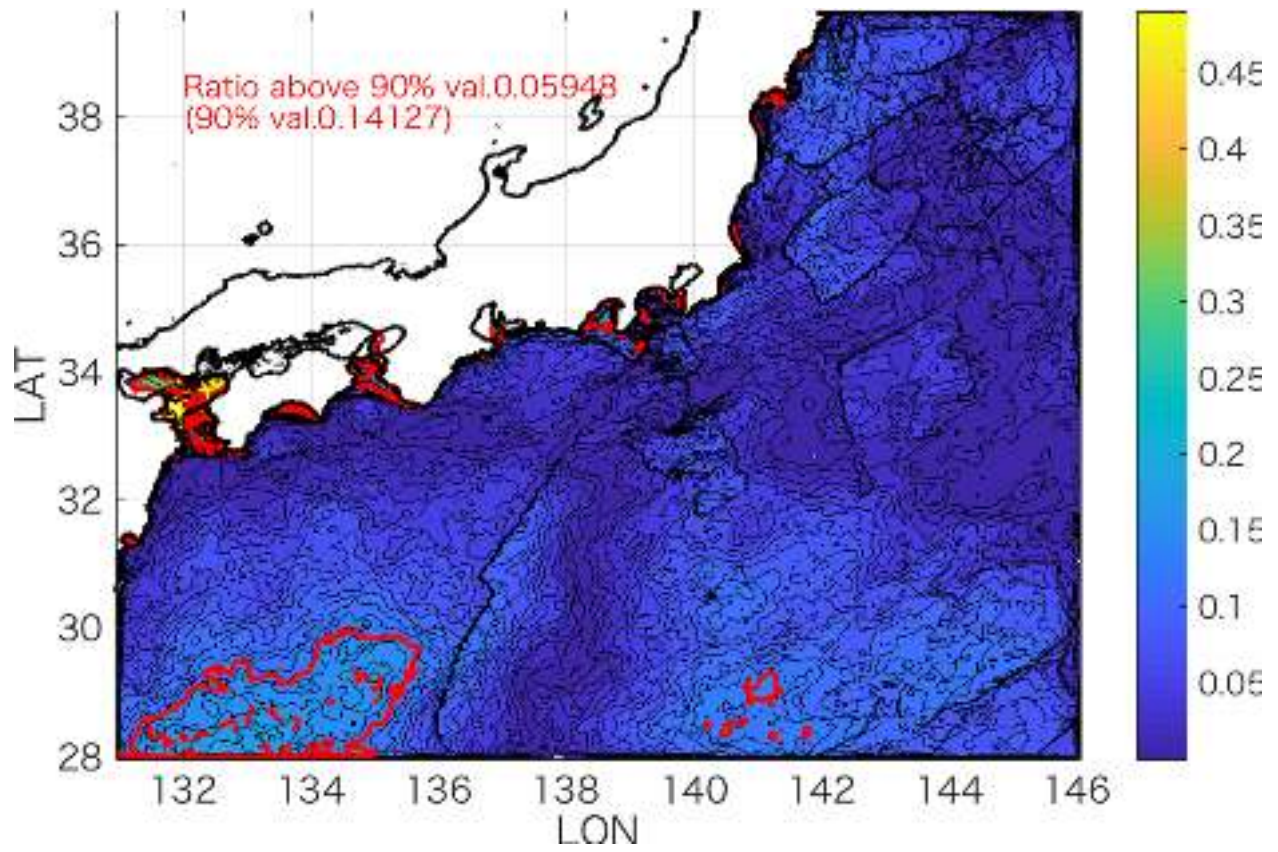


Figure 13: Kendall's tau statistic evaluated for all spatial locations. Red contour encompassed neighbourhoods within which the value of Kendall's tau is unusually large indicating possible dependence between S and E_j .

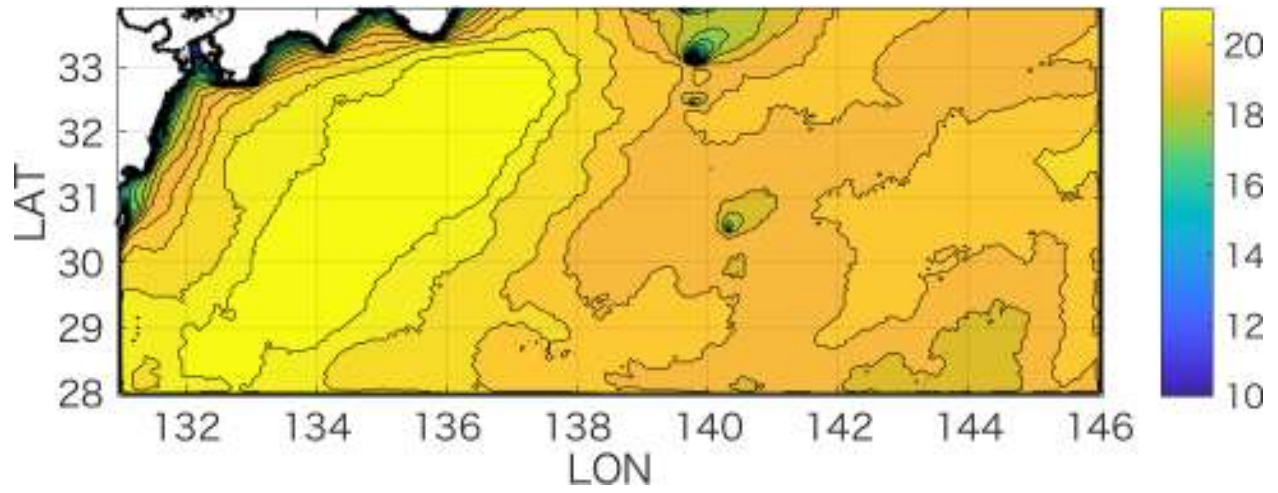


Figure 14: Spatial map of 100-year return value for H_S for medium-sized region B, to be compared with Figure 8.

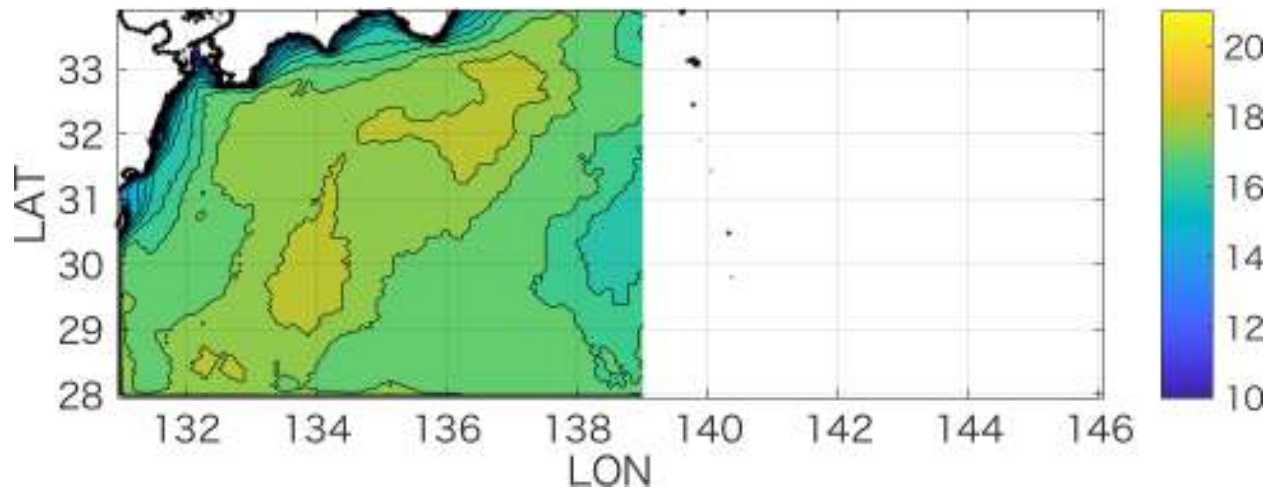


Figure 15: Spatial map of 100-year return value for H_S for small region C, to be compared with Figure 8.

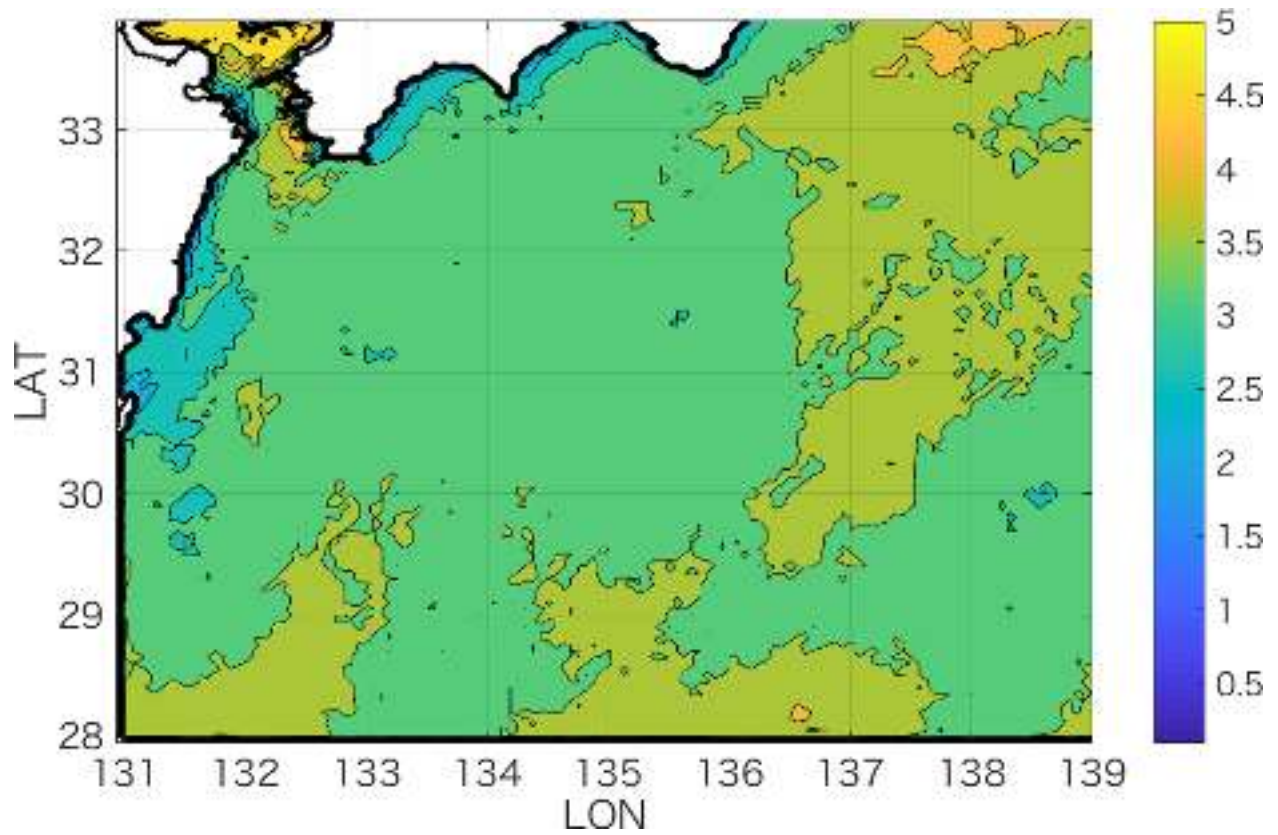


Figure 16: 2.5%ile of bootstrap uncertainty distribution based on bootstrap analysis of full spatial domain A, focussed on region C for comparison with Figure 15.

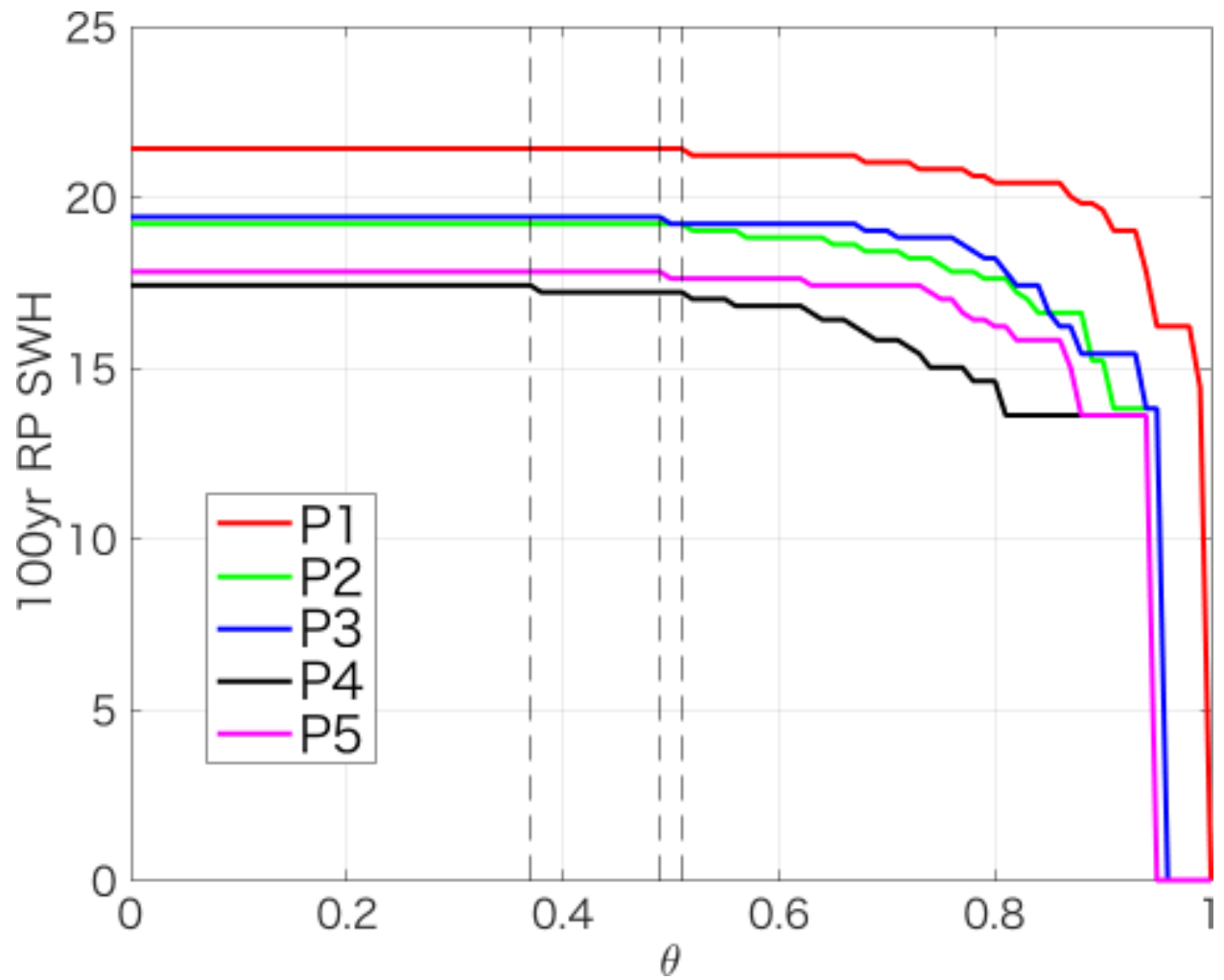


Figure 17: Effect of truncation of distribution of exposure E at probability level θ for each of the five locations P1-P5.

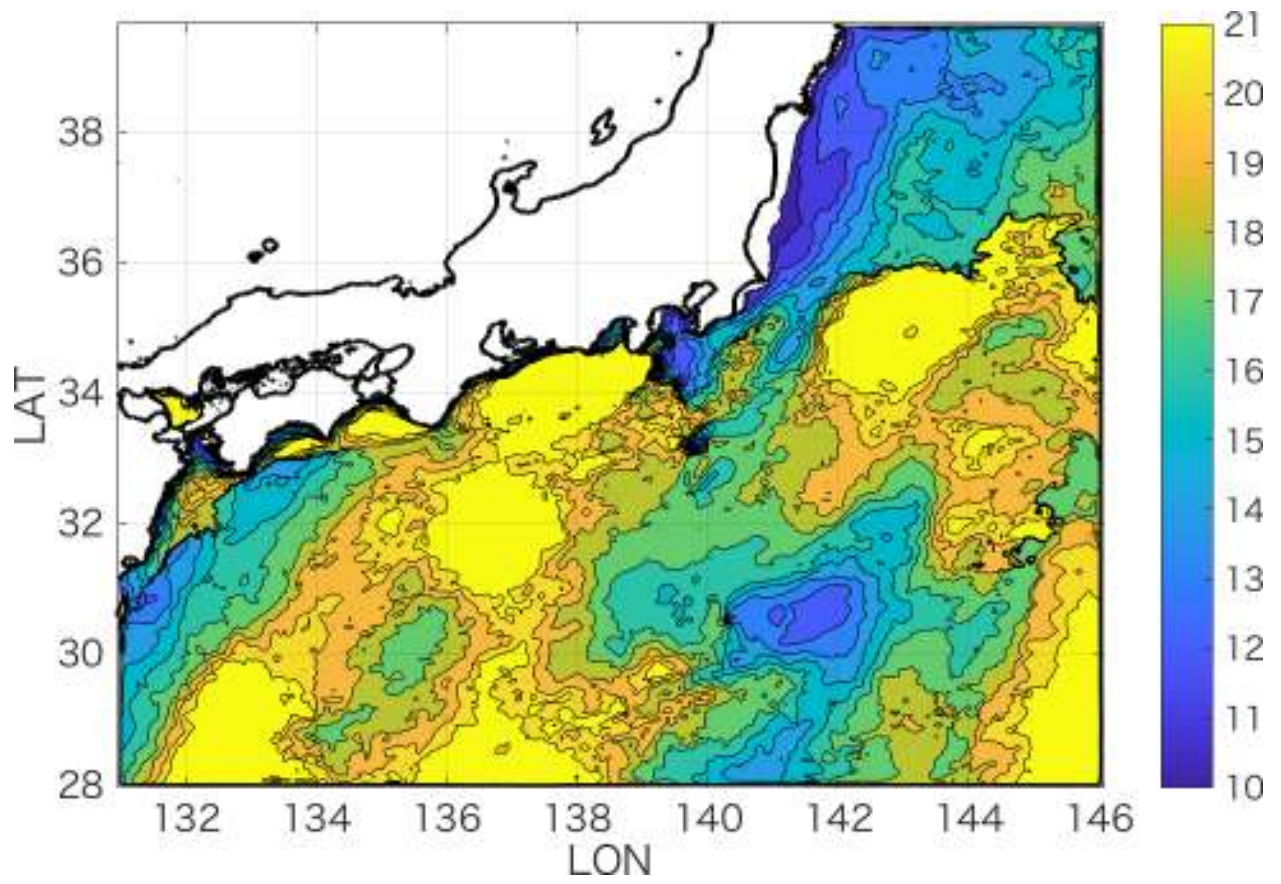


Figure 18: 100-year return value estimates for H_S per location estimated from single point analysis.

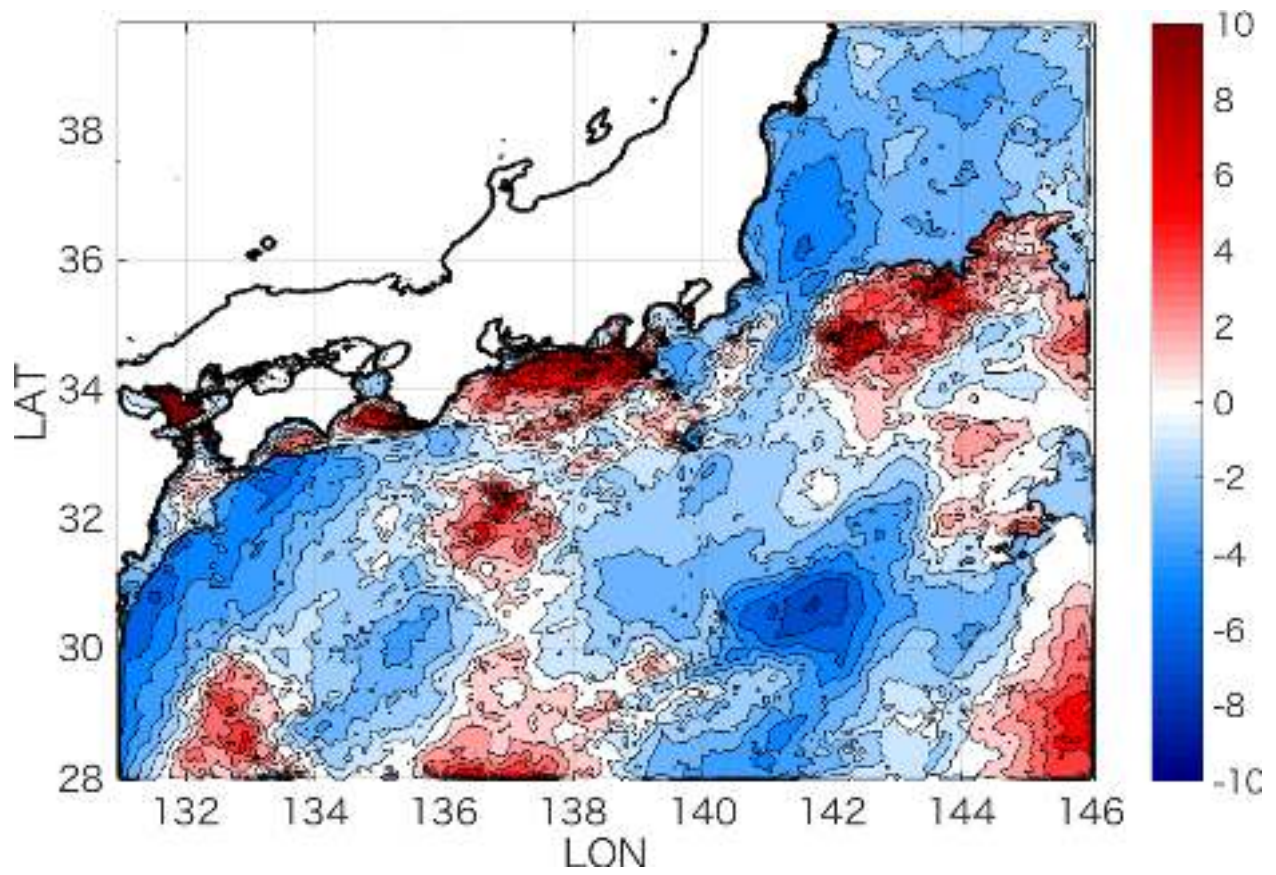


Figure 19: Difference between 100-year return value estimates for H_S per location estimate from single point analysis, and that estimated using the STM-E spatial model.

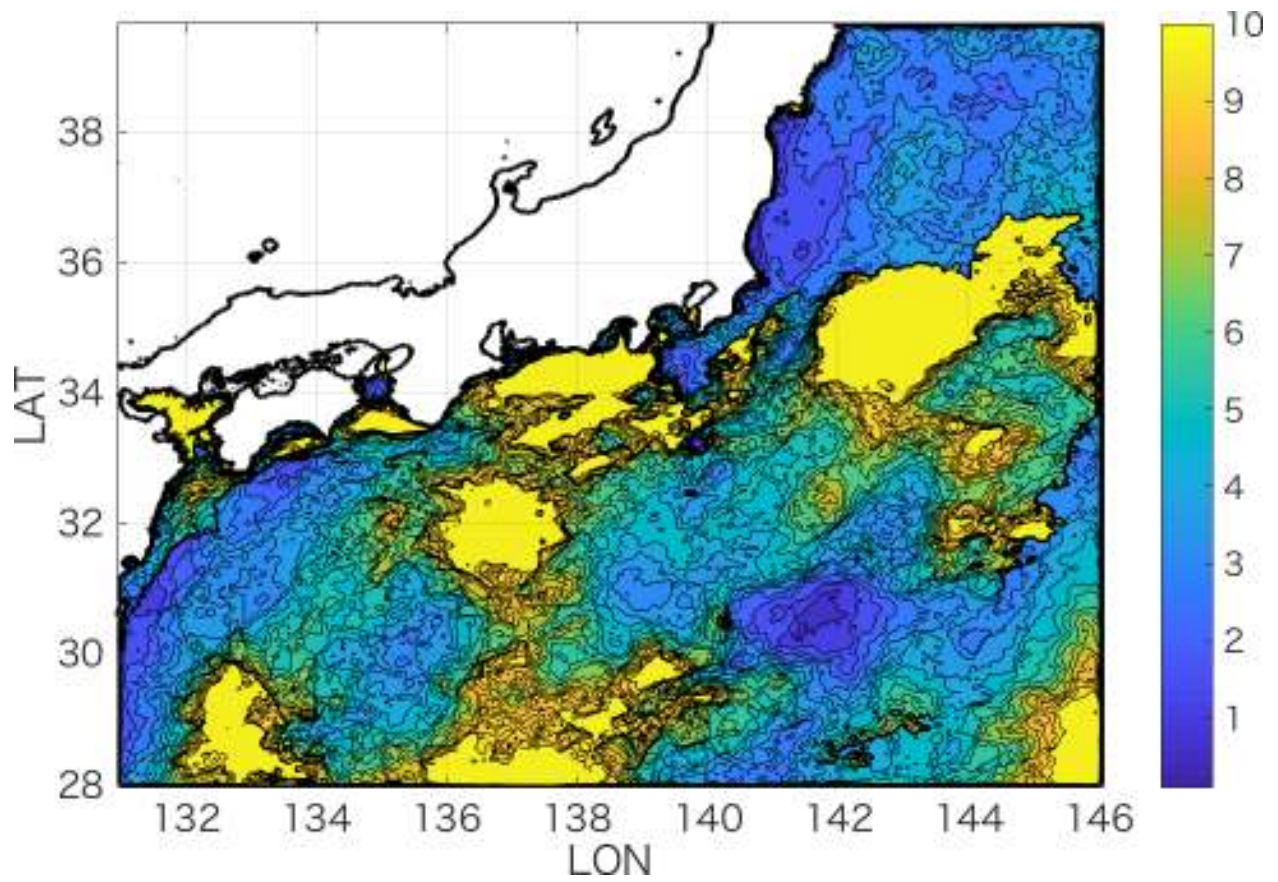


Figure 20: Interquartile range from distribution of the 100-year maximum event from single point analysis. Note, for ease of comparison with Figure 21, that values of interquartile range exceeding 10m are truncated at 10m here. The full distribution of interquartile range is shown in Figure 22.

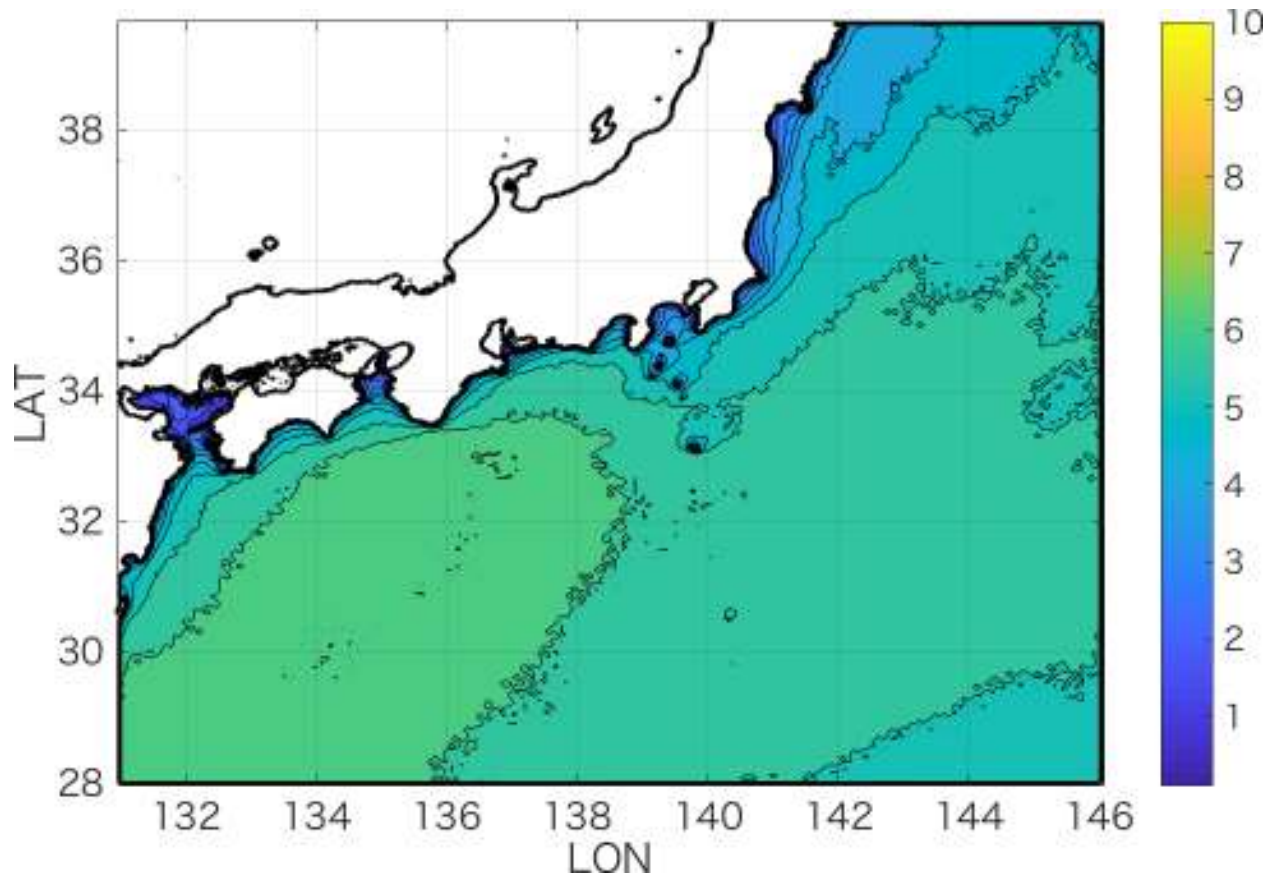


Figure 21: Interquartile range from distribution of the 100-year maximum event from STM-E spatial model, using same colour scale as Figure 20.

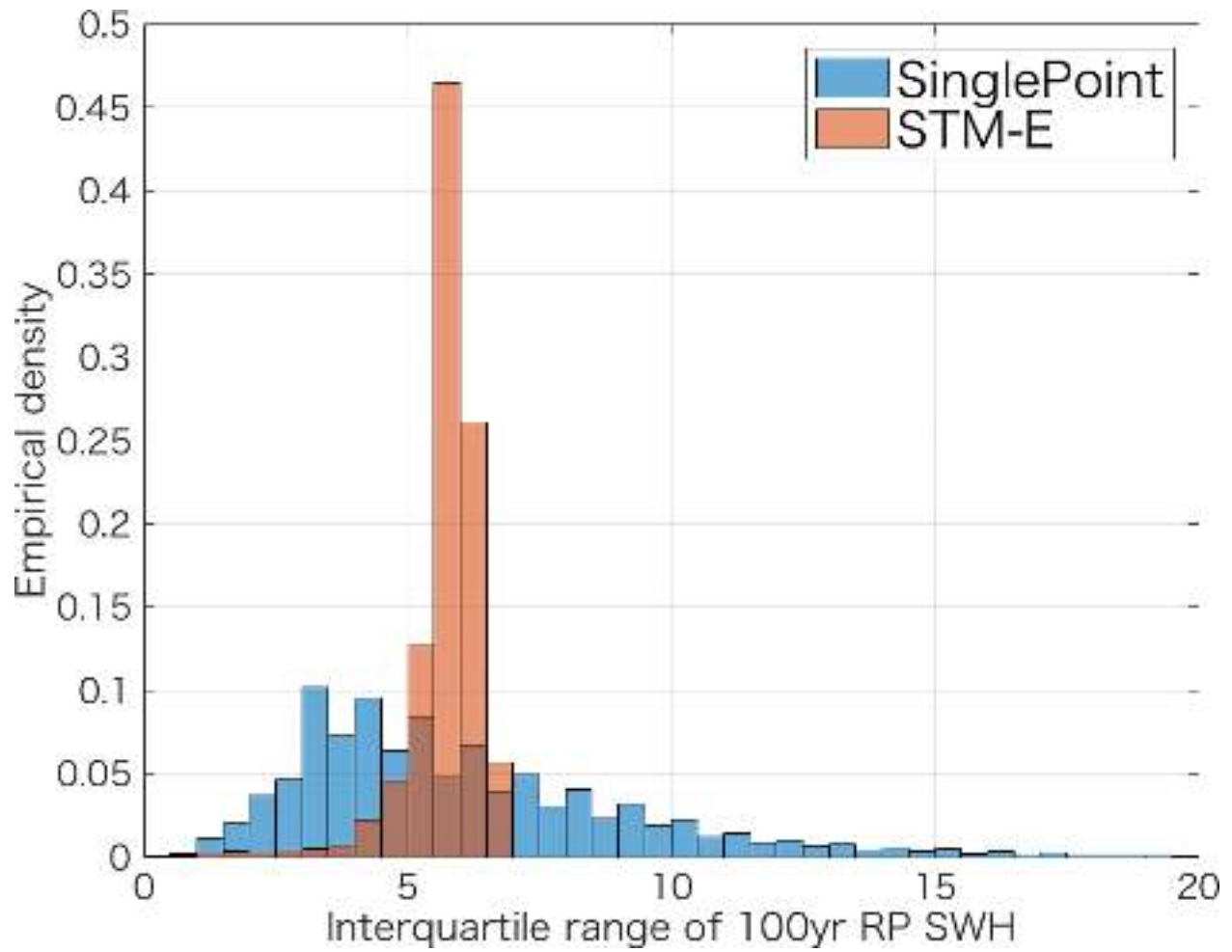


Figure 22: Empirical densities for the interquartile range of the distribution of the 100-year maximum event from single point and STM-E estimates illustrated spatially in Figure 20 and Figure 21.

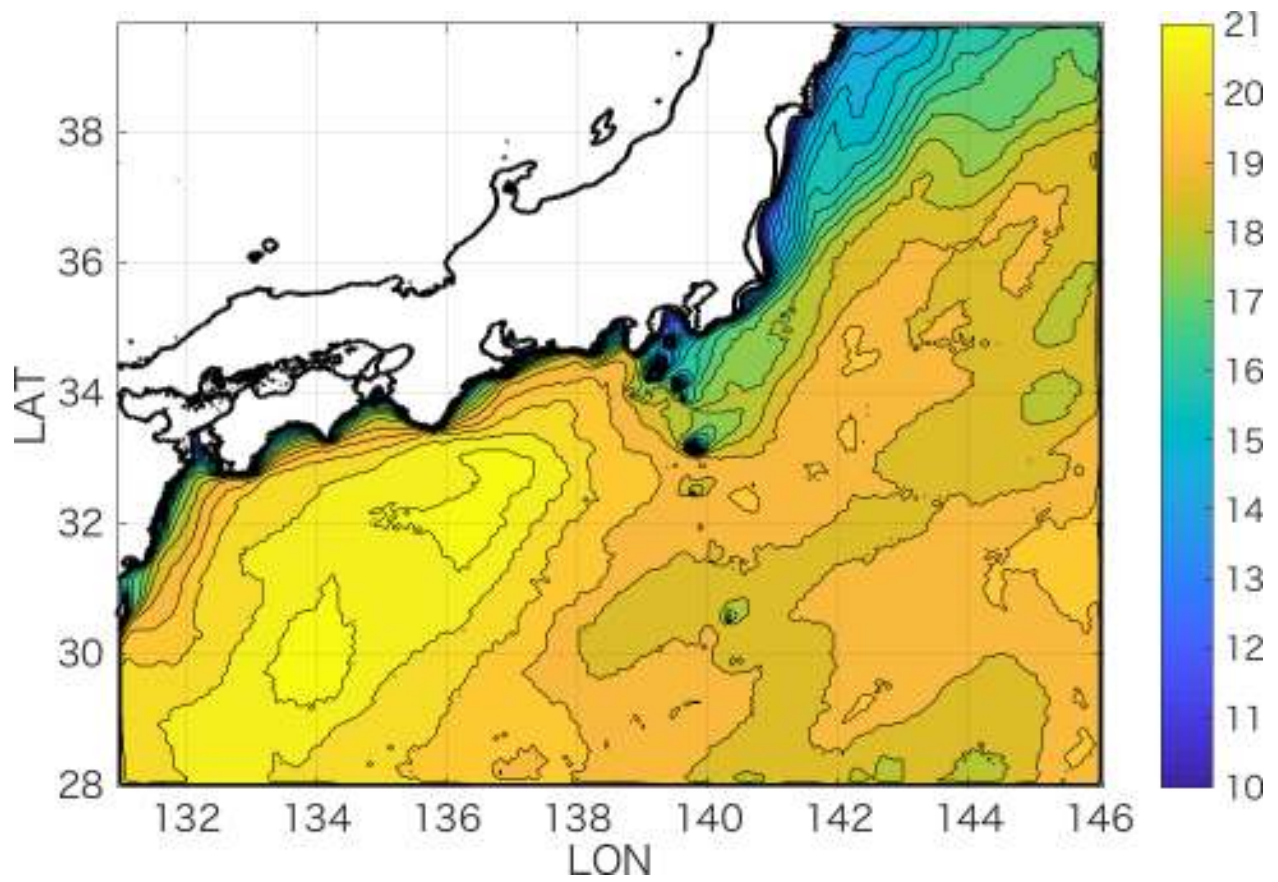


Figure 23: Spatial map of 100-year return value for H_s using 5m peak-picking threshold, to be compared with Figure 8.

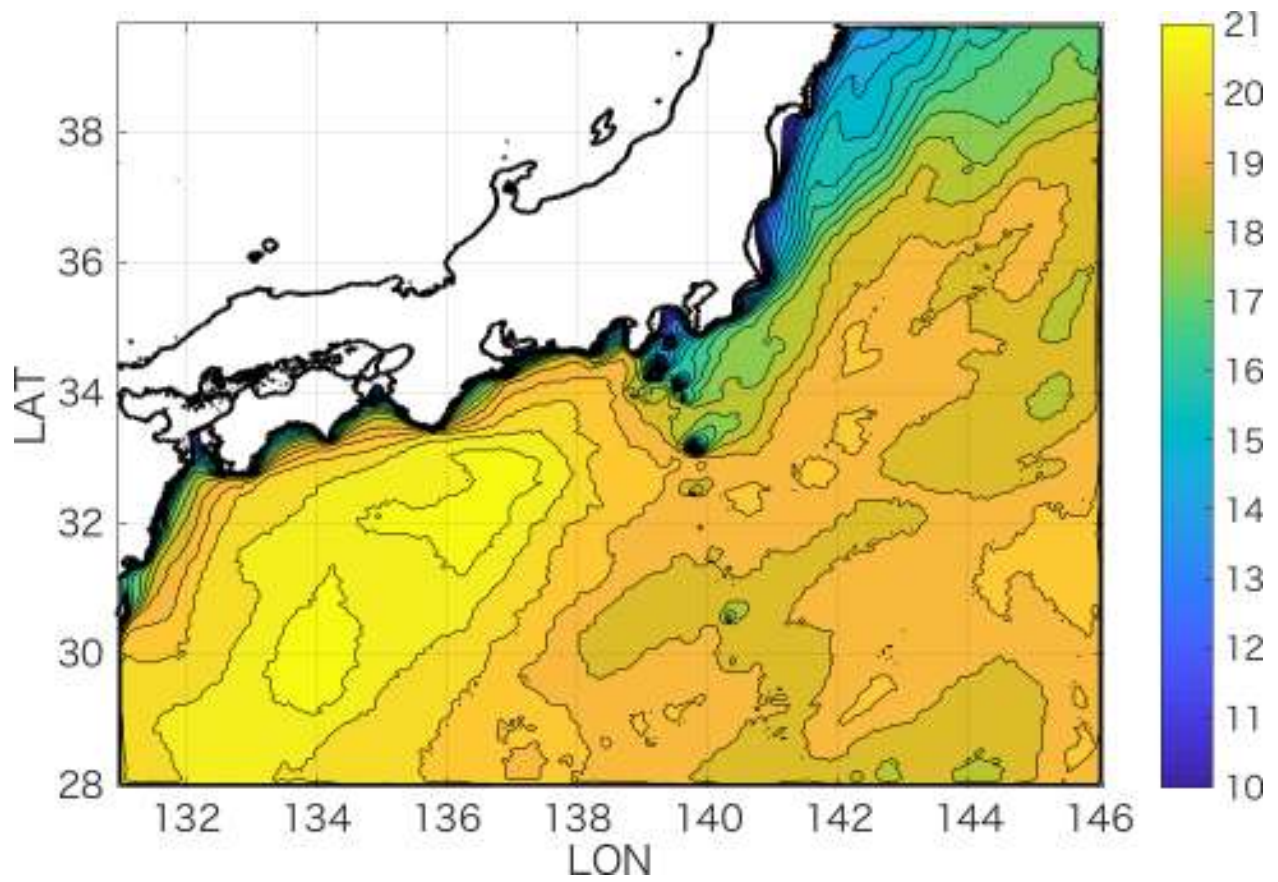


Figure 24: Spatial map of 100-year return value for H_s using 3 day peak merge interval, to be compared with Figure 8.

List of Tables

- 1 Comparison of interquartile ranges (in metres) for the bootstrap distribution of 100-year return value for H_S , considering (column “STM-E”) bootstrap variability in both STM and exposure, and (column “Exposure only”) bootstrap uncertainty in exposure, but no bootstrap uncertainty in STM. 48

Table 1: Comparison of interquartile ranges (in metres) for the bootstrap distribution of 100-year return value for H_S , considering (column “STM-E”) bootstrap variability in both STM and exposure, and (column “Exposure only”) bootstrap uncertainty in exposure, but no bootstrap uncertainty in STM.

Location	STM-E	Exposure only
Point 1	2.2	0.8
Point 2	1.7	0.8
Point 3	1.9	0.8
Point 4	1.9	1.0
Point 5	1.5	0.8